AD-A096 072 CALIFORNIA UNIV SAN DIEGO LA JOLLA DEPT OF CHEMISTRY F/G 7/4
MOLECULAR DYNAMICS AND SPECTRA. II. DIATOMIC RAMAN.(U)
FEB 81 K R WILSON, P H BERENS, S R WHITE N00014-78-C-0325
UNCLASSIFIED TR-3 NL

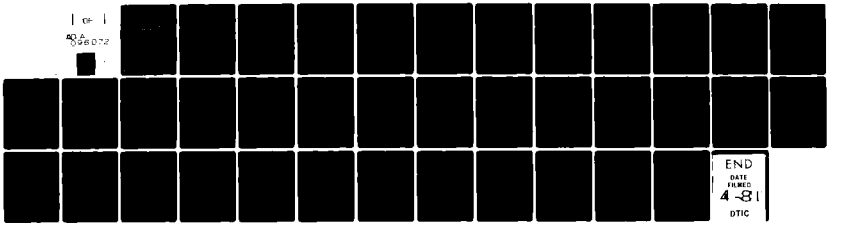

AD A096072

DDC FILE_COPY

REPORT DOCUMENTATION PAGE

READ INSTRUCTIONS BEFORE COMPLETING FORM

1. REPORT NUMBER: 3	2. GOVT ACCESSION NO.: AD-A096072
3. RECIPIENT'S CATALOG NUMBER: 9	
4. TITLE (and Subtitle): MOLECULAR DYNAMICS AND SPECTRA. II. DIATOMIC RAMAN,	5. TYPE OF REPORT & PERIOD COVERED: Technical Report,
	6. PERFORMING ORG. REPORT NUMBER
7. AUTHOR(S): Kent R./Wilson, Peter H./Berens, Steven R./White	8. CONTRACT OR GRANT NUMBER(S): 15 ONR-N00014-78 C-0325
9. PERFORMING ORGANIZATION NAME AND ADDRESS: Department of Chemistry, University of California, San Diego, La Jolla, CA 92093	10. PROGRAM ELEMENT, PROJECT, TASK AREA & WORK UNIT NUMBERS: 14 TR-3
11. CONTROLLING OFFICE NAME AND ADDRESS: Office of Naval Research, Arlington, VA 22217	12. REPORT DATE: Feb[illegible] 1981
	13. NUMBER OF PAGES
14. MONITORING AGENCY NAME & ADDRESS (if different from Controlling Office): 12/38	15. SECURITY CLASS. (of this report): Unclassified
	15a. DECLASSIFICATION/DOWNGRADING SCHEDULE

LEVEL II

16. DISTRIBUTION STATEMENT (of this Report)

This document has been approved for public release and sale; its distribution is unlimited.

17. DISTRIBUTION STATEMENT (of the abstract entered in Block 20, if different from Report)

MAR 1981

18. SUPPLEMENTARY NOTES

Prepared for publication in the Journal of Chemical Physics

19. KEY WORDS (Continue on reverse side if necessary and identify by block number)

molecular dynamics
spectra, Raman
array processor
computer simulation
diatomic rotation and vibration

20. ABSTRACT (Continue on reverse side if necessary and identify by block number)

This paper and Paper I in this series (P.H. Berens and K.R. Wilson, J. Chem. Phys., in press) indicate that infrared and Raman rotational and fundamental vibrational-rotational spectra of dense systems (high pressure gases, liquids and solids) are essentially classical, in that they can be computed and understood from a basically classical mechanical viewpoint, with some caveats for features in which anharmonicity is important, such as the detailed shape of Q branches. It is demonstrated here, using the diatomic

DD FORM 1 JAN 73 1473 EDITION OF 1 NOV 65 IS OBSOLETE
S/N 0102 LF 014 6601

SECURITY CLASSIFICATION OF THIS PAGE (When Data Entered)

400410

20. ABSTRACT (continued)

case as an example, that ordinary, i.e. nonresonant, Raman band contours can be computed from classical mechanics plus simple quantum corrections. Classical versions of molecular dynamics, linear response theory and ensemble averaging, followed by straightforward quantum corrections, are used to compute the pure rotational and fundamental vibrational-rotational Raman band contours of N_2 for the gas phase and for solutions of N_2 in different densities of gas phase Ar and in liquid Ar. The evolution is seen from multiple peaked line shapes characteristic of free rotation in the gas phase to single peaks characteristic of hindered rotation in the liquid phase. Comparison is made with quantum and correspondence principle classical gas phase spectral calculations and with experimental measurements for pure N_2 and N_2 in liquid Ar. Three advantages are pointed out for a classical approach to infrared and Raman spectra. First, a classical approach can be used to compute the spectra of complex molecular systems, for example of large molecules, clusters, liquids, solutions, and solids. Second, this classical approach can be extended to compute the spectra of non-equilibrium and time-dependent systems, for example infrared and Raman spectra during the course of chemical reactions. Third, a classical viewpoint allows experimental infrared and Raman spectra to be understood and interpreted in terms of atomic motions with the considerable aid of classical models and of our well-developed classical intuition.

OFFICE OF NAVAL RESEARCH

Contract N00014-78 C-0525

TECHNICAL REPORT NO.3

Molecular Dynamics and Spectra.

II. Diatomic Raman

by

Kent R. Wilson, Peter H. Berens and Steven R. White

Prepared for Publication

in the

Journal of Chemical Physics

University of California, San Diego

Department of Chemistry

La Jolla, CA 92093

February, 1981

MOLECULAR DYNAMICS AND SPECTRA. II. DIATOMIC RAMAN

Peter H. Berens, Steven R. White and Kent R. Wilson

Department of Chemistry
University of California, San Diego
La Jolla, CA 92093

ABSTRACT

This paper and Paper I in this series (P. H. Berens and K. R. Wilson, *J. Chem. Phys.*, in press) indicate that infrared and Raman rotational and fundamental vibrational-rotational spectra of dense systems (high pressure gases, liquids and solids) are essentially classical, in that they can be computed and understood from a basically classical mechanical viewpoint, with some caveats for features in which anharmonicity is important, such as the detailed shape of Q branches. It is demonstrated here, using the diatomic case as an example, that ordinary, *i.e.* nonresonant, Raman band contours can be computed from classical mechanics plus simple quantum corrections. Classical versions of molecular dynamics, linear response theory and ensemble averaging, followed by straightforward quantum corrections, are used to compute the pure rotational and fundamental vibrational-rotational Raman band contours of N_2 for the gas phase and for solutions of N_2 in different densities of gas phase Ar and in liquid Ar. The evolution is seen from multiple peaked line shapes characteristic of free rotation in the gas phase to single peaks characteristic of hindered rotation in the liquid phase. Comparison is made with quantum and correspondence principle classical gas phase spectral calculations and with experimental measurements for pure N_2 and N_2 in liquid Ar. Three advantages are pointed out for a classical approach to infrared and Raman spectra. First, a classical approach can be used to compute the spectra of complex molecular systems, for example of large molecules, clusters, liquids, solutions, and solids. Second, this classical approach can be extended to compute the spectra of nonequilibrium and time-dependent systems, for example infrared and Raman spectra during the course of chemical reactions. Third, a classical viewpoint allows experimental infrared and Raman spectra to be understood and interpreted in terms of atomic motions with the considerable aid of classical models and of our well-developed classical intuition.

Submitted to *J. Chem. Phys.* February 1981

PACS numbers 33.70.-w, 33.20.Fb, 33.10.Jz, 78.30.Cp

MOLECULAR DYNAMICS AND SPECTRA. II. DIATOMIC RAMAN

Peter H. Berens, Steven R. White and Kent R. Wilson

Department of Chemistry
University of California, San Diego
La Jolla, CA 92093

I. INTRODUCTION

The properties of matter and the processes it undergoes are determined not just by its average structure but also by its dynamics, its time evolution. Thus to understand these properties and processes we would like a window through which to observe atomic motions. As Gordon has emphasized,[1] infrared and Raman spectra intimately reflect both intra- and intermolecular motions, and thus in principle can provide such a window. In practice, if we use quantum mechanics as our link between time evolution and spectra, we are limited to the analysis of rather simple cases by computational complexity and by our inability to easily conceptualize in a quantum framework. Semiclassical approaches can carry us further, but not as yet far enough to handle more than simple systems. Thus a generalized classical approach which could successfully link molecular dynamics and infrared and Raman spectra would be very useful, for example in discovering the dynamics underlying liquid properties, or in following chemical change in condensed phases.

In the first paper [2] of this series, which we will henceforth call Paper I, we demonstrated for a diatomic molecule that pure rotational and fundamental vibrational-rotational infrared band contours can be computed from classical mechanics plus simple quantum corrections. In this paper we apply the same classical approach of molecular dynamics, linear response, and ensemble averaging, followed by simple quantum corrections, to compute diatomic pure rotational and vibrational-rotational Raman spectra. While one could introduce aspects of quantum mechanics directly into the dynamics, and thus adopt a semiclassical molecular dynamics approach,[1,3-12] we illustrate that the spectra are so very nearly classical that a much simpler approach is usually quite adequate, one in which the introduction of quantum mechanics is delayed until the end and then the final classical spectra are quantum corrected. We demonstrate that this technique, which we call a "Newtonian" approach to emphasize its basically classical nature, allows the computation of diatomic pure rotational and fundamental vibrational-rotational Raman spectral band contours. In order that rigorous tests may be made versus other theoretical approaches and experiment, we have chosen to treat a molecular system, N_2 in the gas phase and its solution in Ar, which is quite simple. Nevertheless, one of the virtues of the Newtonian approach to infrared and Raman spectra is the relative ease with which it can be extended to more complex systems, such as molecular clusters, large molecules, liquids, solutions, and solids, as well as to non-equilibrium and time-dependent systems.[13] In order to demonstrate this approach and to develop the necessary quantum corrections, we compare theoretical spectra computed in three different ways: *i)* quantum mechanics without linear response theory, *ii)* correspondence principle classical mechanics without linear response theory, *i.e* the limit of quantum mechanics as Planck's constant approaches zero, and *iii)* ordinary Newtonian classical mechanics with classical linear response theory and ensemble averaging from classical statistical mechanics. In addition, we compare with several experimental spectra for pure N_2 and for N_2 in Ar.

II. THEORETICAL TECHNIQUES

We use the same basic Newtonian theoretical approach presented in Paper I. First, classical mechanics is used to compute the time evolution, *i.e.* the atomic trajectories, of the system of interest from a set of initial atomic positions and velocities and a given potential surface. Second, the time varying polarizability matrix for the entire system of molecules is calculated from the atomic trajectories. Third, linear response theory, as applied to Raman spectra by Gordon,[1,14-17] is used to calculate a "specific" Raman spectrum for each molecular dynamics run. Fourth, these "specific" spectra are averaged over an ensemble appropriate to the experimental conditions of interest through the choice of different sets of initial positions and velocities for a series of molecular dynamics runs. Fifth, quantum corrections are applied where necessary to the purely classical spectrum to converge toward the real quantum spectrum.

In Paper I we showed that a similar set of five steps produce surprisingly accurate infrared spectra. We show here that Raman spectra are also well reproduced in this way, using as inputs only the potential energy $V(\mathbf{r})$ and the polarizability $\bar{\mathbf{P}}(\mathbf{r})$ as functions of nuclear positions. Since the main aim of this paper is to show that relatively simple classical techniques and quantum corrections can reproduce quantum reality for Raman spectra, we have relegated to a series of appendices most of the complexity of the quantum treatment, which we need to derive quantum corrections and to demonstrate by comparing classical and quantum spectra that a simpler classical approach indeed works. These appendices can be skipped by those readers only interested in the classical results.

A. Molecular dynamics and classical trajectories

Given appropriate inter- and intra-molecular potentials to describe the interactions among atoms, molecular dynamics can be used to calculate from a set of initial positions and velocities the time evolution of the system of interest. Computation of the classical trajectories $\mathbf{r}_1(t), \ldots, \mathbf{r}_N(t)$ for a system of N atoms involves numerically integrating the N coupled differential equations given by Newton's Second Law

$$-\frac{\partial V}{\partial \mathbf{r}_i} = \mathbf{F}_i = m_i \frac{d^2\mathbf{r}_i}{dt^2}, \quad i = 1, \ldots, N \tag{1}$$

in which $V = V(\mathbf{r}_1, \ldots, \mathbf{r}_N)$ is the potential energy of the atoms (or more accurately the nuclei) at positions $\mathbf{r}_1, \ldots, \mathbf{r}_N$, $\mathbf{F}_i = \mathbf{F}_i(\mathbf{r}_1, \ldots, \mathbf{r}_N)$ is the force on the ith atom, and m_i is its mass. A modified Verlet integration algorithm is used.[18,19] For the case below of an N_2 solution in Ar, minimum image periodic boundary conditions with truncated octahedral boundaries[20] and forces smoothly feathered to zero over the outer 0.01 nm of the radius of the inscribed sphere (which, for the cases considered here, is always greater than 0.57 nm) are used to reduce edge effects.

This type of calculation, while straightforward in concept, can be extremely demanding arithmetically. We have built an "instrument for theory", partially described elsewhere,[21] which consists of a generalized program package and a network of computers including an array processor and a three dimensional display processor. This instrument allows us to compute spectral and other properties of even rather large and complex molecular systems.

B. Time history of the polarizability

Given the Cartesian tensor $\bar{\mathbf{P}}(\mathbf{r}_1, \ldots, \mathbf{r}_N)$ which describes the polarizability in space-fixed coordinates of the system as a function of atomic positions, we use the trajectories of the atoms, $\mathbf{r}_1(t), \ldots, \mathbf{r}_N(t)$, calculated from molecular dynamics to compute $\bar{\mathbf{P}}(t)$, the polarizability tensor of the system as a function of time. Polarizability tensors in molecule or bond fixed coordinate systems are transformed into space fixed coordinates by the use of direction cosines.[22]

C. Linear response and specific spectra

Gordon[1,14,16] has shown that linear response theory (see Appendices A and B) can be used to compute the Raman spectrum by relating the spectrum of fluctuations which the polarizability tensor $\bar{\mathbf{P}}(t)$ naturally undergoes when the system is free of outside perturbation to the spectrum of the Raman scattered light which $\bar{\mathbf{P}}(t)$ produces when the system is driven by the oscillating electric field of light.

From Appendices A and B, the appropriate linear response equations are

$$\left(\bar{\nu}_s^4 \frac{d^2\sigma}{d\omega d\Omega}\right)_{iso} = \frac{1}{2\pi} \int_{-\infty}^{\infty} dt \; e^{-i\omega t} \; \tfrac{1}{3} <\mathrm{Tr}[\bar{\mathbf{P}}_{iso}(0)\, \bar{\mathbf{P}}_{iso}(t)]> \tag{2}$$

$$\left(\bar{\nu}_s^4 \frac{d^2\sigma}{d\omega d\Omega}\right)_{aniso} = \frac{1}{2\pi} \int_{-\infty}^{\infty} dt \; e^{-i\omega t} \; <\mathrm{Tr}[\bar{\mathbf{P}}_{aniso}(0)\, \bar{\mathbf{P}}_{aniso}(t)]> \tag{3}$$

in which the left hand sides of Eqs. (2) and (3) are the differential cross sections for scattering into angular frequency range $d\omega$ and solid angle range $d\Omega$ for the isotropic and anisotropic Raman spectra, respectively, weighted by $\bar{\nu}_s^4$ in which $2\pi\bar{\nu}_s$ is the wavelength of the scattered radiation. The $\bar{\mathbf{P}}_{iso}$ and $\bar{\mathbf{P}}_{aniso}$ are the isotropic and anisotropic parts of the polarizability tensor of the system, respectively, as defined in Eqs. (A2)-(A4) of Appendix A. Tr indicates the trace and $< >$ indicates an ensemble average.

As Parseval's theorem[23] and the Wiener-Khintchine theorem[17,24,25] show, the Raman cross sections given above as Fourier transforms of time correlation functions may also be computed in the mathematically equivalent form of power spectra,

$$\left(\bar{\nu}_s^4 \frac{d^2\sigma}{d\omega d\Omega}\right)_{iso} = \frac{1}{2\pi} \left[\lim_{\tau\to\infty} \frac{1}{2\tau} \left| \int_{-\tau}^{\tau} dt \; e^{-i\omega t} \, \tfrac{1}{3} \,\mathrm{Tr}\, \bar{\mathbf{P}}(t) \right|^2 \right] \tag{4}$$

$$\left(\bar{\nu}_s^4 \frac{d^2\sigma}{d\omega d\Omega}\right)_{aniso} = \frac{1}{2\pi} \sum_{ij} \left[\lim_{\tau\to\infty} \frac{1}{2\tau} \left| \int_{-\tau}^{\tau} dt \; e^{-i\omega t} \, [\bar{\mathbf{P}}_{aniso}]_{ij}(t) \right|^2 \right], \tag{5}$$

allowing the use of fast Fourier techniques. Considerable care must be used to properly apply spectral estimation theory, windowing and windowing corrections,[2,23,26] in both the correlation and power spectrum methods to avoid distorting the spectra as a result of the use of finite time histories. Particular care must be taken if band wings are to be correct or if small bands are to be seen in the presence of large ones. We use a four term −74 db Blackman-Harris window,[26] which allows the correction to be applied as a simple frequency-space convolution of the Fourier transform of the polarizability matrix element time histories with the Fourier transform of the window function, in a parallel manner to that described in Paper I. The time correlation functions can then be computed, if desired, from the Fourier inverses of Eqs. (2) and (3). In this way spectral estimation theory is correctly used, undesirable distortions in the correlation functions from finite time histories are avoided, and the speed advantage of fast Fourier techniques is retained.[24,25]

The isotropic and anisotropic cross sections may be related to the usual experimental parallel and perpendicular spectra by[16,17,22]

$$\left(\bar{\nu}_s^4 \frac{d^2\sigma}{d\omega d\Omega}\right)_{\parallel} = \left(\bar{\nu}_s^4 \frac{d^2\sigma}{d\omega d\Omega}\right)_{iso} + \frac{2}{15} \left(\bar{\nu}_s^4 \frac{d^2\sigma}{d\omega d\Omega}\right)_{aniso} \tag{6}$$

$$\left(\bar{\nu}_s^4 \frac{d^2\sigma}{d\omega d\Omega}\right)_{\perp} = \frac{1}{10} \left(\bar{\nu}_s^4 \frac{d^2\sigma}{d\omega d\Omega}\right)_{aniso}. \tag{7}$$

D. Ensemble averaging

Since a specific spectrum is computed from a single molecular dynamics run representing only a small portion of phase space, in order to compute a spectrum comparable to an experimental spectrum taken, for example, at a particular temperature and pressure, it is necessary to average the specific spectra over an ensemble of runs with properly chosen different initial positions and velocities. To provide a sufficiently accurate ensemble average we must insure that enough of phase space is sampled. Thus, to begin a spectral computation we choose reasonable guesses for the initial positions $\mathbf{r}_1(0), \ldots, \mathbf{r}_N(0)$ and equilibrate the system to the temperature of interest. We integrate forward in time, stopping at intervals to choose a new set of velocities selected randomly from a Maxwell-Boltzmann distribution. After the system is sufficiently equilibrated, we begin taking specific spectra. The final positions of the molecular dynamics run for the previous specific spectrum are used as the initial positions for the next run, in an attempt to sample more of configuration space by allowing slow rearrangements in configuration space to accumulate. Because for weakly interacting systems such as dilute gases, constants of the motion for individual molecules such as angular momentum are conserved over long periods (nonergodicity), and thus even long molecular dynamics runs will sample only restricted regions of phase space, it is necessary to introduce some stochastic element into the deterministic molecular dynamics. Therefore, we randomly pick a new set of velocities from the Maxwell-Boltzmann distribution at the beginning of each run. While this is necessary for weakly interacting systems, it may contribute little to strongly interacting ones in which the velocity autocorrelation function dies off quickly, and, by turning concerted motion through configuration space into diffusive motion, it might even slow down the convergence to a proper configuration space average if applied too frequently.[19]

E. Potential and polarizability functions

The intramolecular potential function used for N_2 is a fourth order Taylor's series expansion about the equilibrium bond distance[27] of 0.109768 nm. The potential derivatives, V'', V''', and V'''', at the equilibrium bond distance, listed in Table I, are derived using Eqs. (C21)-(C26) from the ground state spectral constants listed by Huber and Herzberg.[27]

TABLE I. Potential function parameters for N_2

V'' (Jm^{-2})	V''' (Jm^{-3})	V'''' (Jm^{-4})
2.295×10^{3}	-1.696×10^{14}	9.980×10^{24}

We have used as the polarizabilities for N_2 the values shown in Table II, where, for a diatomic in molecule fixed coordinates, $\bar{P}''_{zz}$ and $\bar{P}''_{xx}=\bar{P}''_{yy}$ are the parallel and perpendicular components, respectively, and α''_{iso} and α''_{aniso} are the isotropic and anisotropic polarizability components, respectively, given by Eqs. (A9) and (A10) of Appendix A. The linear expansion given by Eqs. (A29) and (A30) is used.

TABLE II. Polarizabilities for N_2

$\bar{P}''_{zz}$	$\bar{P}''_{xx}$	α''_{iso}	α''_{aniso}	$\bar{P}'_{zz}$	$\bar{P}'_{xx}$	α'_{iso}	α'_{aniso}
($10^{-30}m^3$)				($10^{-30}m^2$)			
2.196	1.512	1.740	0.558	2.67	1.27	1.74	1.14

The values of $\bar{P}''_{zz}$, $\bar{P}''_{xx}$, α''_{iso}, and α''_{aniso} are the experimental values adopted by Morrison and Hay.[28,33] The values of $\bar{P}'_{zz}$, $\bar{P}'_{xx}$, α'_{iso}, and α'_{aniso} are derived from the value for α'_{aniso} after Asawaroengchai *et. al.*[34] combined with the value of the absolute differential Raman scattering cross section for the fundamental vibrational-rotational Q branch of N_2 given by Schrötter and Klöckner[35] using Eqs. (C16) and (C17).

F. Quantum corrections

In order to discover what corrections are necessary to bring our classical calculations into agreement with quantum reality, we compare in Appendix E two different ways of computing the Raman spectrum: *i*) quantum mechanics without linear response theory, and *ii*) correspondence principle classical mechanics without linear response theory as given by the limit of quantum mechanics as Planck's constant approaches zero. Our Newtonian classical mechanics with classical linear response theory and ensemble averaging from classical statistical mechanics should agree with correspondence principle classical mechanics if both are carried out accurately, and thus if we learn to properly quantum correct one we can also correct the other.

1. Pure rotational bands

The detailed balance correction to the pure rotational band is given in Eq. (E5) of Appendix E as

$$\left[\tilde{\nu}_s^4 \frac{d^2\sigma}{d\omega d\Omega}\right]_Q^R \Big/ \left[\tilde{\nu}_s^4 \frac{d^2\sigma}{d\omega d\Omega}\right]_C^R = \exp(\beta\hbar\omega/2) \tag{8}$$

in which the superscript R indicates rotational and the subscripts Q and C indicate quantum and classical, respectively. In Eq. (8), $\beta=(k_B T)^{-1}$ in which k_B is Boltzmann's constant and T the temperature. This correction can be understood by considering that in the correspondence principle limit as $\hbar\to 0$ and as quantum mechanics converges toward classical mechanics, Raman scattering at frequency ω corresponds to infinitesimally small quanta of energy $\hbar\omega$ and produces transitions between states infinitesimally close in energy, and thus classically of essentially the same statistical probability. Quantum mechanically, lower and upper states are related in probability by the Boltzmann factor $\exp(\beta\hbar\omega)$, and thus Stokes and Antistokes cross sections must be related by this factor. The factor of one half arises from the 2ω separating the Stokes and the Antistokes angular frequencies. Thus we quantum correct a pure rotational band by multiplying it by $\exp(\beta\hbar\omega/2)$.

2. Vibrational-rotational bands

In Appendix D we make the approximation of separating vibration from rotation, and thus we compute the quantum corrections separately, even though in our classical molecular dynamics we make no such separation. The quantum correction for pure harmonic vibration, as given in Eq. (E10) of Appendix E, is an intensity correction

$$\left[\tilde{\nu}_s^4 \frac{d^2\sigma}{d\omega d\Omega}\right]_Q^1 \Big/ \left[\tilde{\nu}_s^4 \frac{d^2\sigma}{d\omega d\Omega}\right]_C^1 = \frac{\beta\hbar\omega}{1-\exp(-\beta\hbar\omega)} . \tag{9}$$

This can be understood by considering that the intensity of Raman scattering is determined by the square of the change in polarizability, which is proportional in the linear approximation used here to the square in the change in bond distance, and thus to the vibrational energy. Quantum mechanically the oscillator energy for $\hbar\omega >> k_B T$ is $\sim\hbar\omega/2$ while classically it is much lower, $\sim k_B T$, and thus the quantum scattering is greater than the classical scattering.

It is also shown in Appendix E that a relatively small frequency shift is needed in order to correct for anharmonicity in the vibrational potential because a classical oscillator samples the potential near the bottom of the well at $\sim k_B T$ where the anharmonicity is smaller than in the region sampled by the zero point and higher quantum states. For the cases we treat here, the anharmonic corrections, calculated as discussed in Appendix E, are -27.2 cm^{-1} at 83 K, -27.0 cm^{-1} at 96 K, and -23.6 cm^{-1} at 298 K. The cruder approximation $-4\pi\nu_e x_e$, using spectral constants from Huber and Herzberg,[27] gives -28.6 cm^{-1}. In addition, if we assume that vibration and rotation are approximately mechanically and thus statistically separable, then the same detailed balance correction given by Eq. (8) needs to be applied within each vibrational band, this time multiplying the band by $\exp[\beta\hbar(\Delta\omega)/2]$, in which $\Delta\omega$ is measured from the rotationless band center.

Therefore the quantum correction of a fundamental vibrational-rotational band consists of three steps. First, the anharmonic offset is computed by the method given in Appendix E and the band is shifted to its quantum corrected position. Second, the band is harmonically corrected by multiplying by the factor given in Eq. (9). Third, the vibrational-rotational band is corrected for detailed balance by multiplication by $\exp[\beta\hbar(\Delta\omega)/2]$, in which $\Delta\omega$ is the angular frequency displacement measured from the rotationless center of the band.

III. SPECTRA

Fig. 1 shows the overall band contour of the N_2 dilute gas phase Raman spectrum which we will now examine in more detail.

A. Gas phase rotational spectra

Fig. 2 shows the anisotropic pure rotational Raman spectrum for gas phase N_2. The isotropic rotational Raman spectrum is zero. Fig. 2 demonstrates that the Raman spectral band contours as computed by *i)* quantum mechanics, using Eq. (C14), *ii)* the quantum corrected correspondence principle, taking the classical $\hbar\rightarrow 0$ limit of Eq. (C14), and *iii)* the quantum corrected Newtonian approach, as given by Eqs. (3) and (5), all agree closely. The quantum spectrum, suitably broadened, also agrees with the experimental results of De Santis *et. al.*[36] The spectral constants for the quantum and correspondence principle calculations are from Huber and Herzberg[27] and the potential energy and polarizability are as described in Tables I and II above. In this, and subsequent figures, the integration step size for the Newtonian molecular dynamics calculations is 5×10^{-16} s.

B. Gas phase vibrational-rotational spectra

Figs. 3 and 4 show the fundamental vibrational-rotational isotropic and anisotropic Raman bands for gas phase N_2. The quantum band contours are calculated from Eqs. (C15)-(C26), the correspondence principle band contours are from the classical limit of Eqs. (C15)-(C26), and the quantum corrected Newtonian band contours are from Eqs. (4) and (5). The potential and polarizability functions are as in the previous section. The finite time step used to obtain the classical trajectories leads to a small offset in the Newtonian vibrational-rotational calculations of $+5.5$ cm^{-1} for which we correct before presenting the spectra. The O ($\Delta J=-2$) and S ($\Delta J=+2$) branch contours are seen in Fig. 4 to agree well among the quantum, quantum corrected correspondence principle classical, and quantum corrected Newtonian approaches. We have not quantum corrected for the effect of anharmonicity on the Q ($\Delta J=0$) line shapes and thus while the Q branch areas agree among the three calculations, the line shape is broader in the correspondence and Newtonian classical calculations than in the real quantum case, as is discussed in Appendix E. The computed quantum Q branch agrees with the experimental measurements of Bendtsen.[37]

C. From gas to liquid

Having demonstrated that the quantum corrected classical approach can provide essentially correct spectral band contours for gas-phase rotational and vibrational-rotational transitions, where we know accurately the potential energy and polarizability functions and where we can compare to accurate quantum calculations, we now turn to higher densities, where our knowledge of the potential energy and polarizability functions is less certain, and our ability to compute spectra by alternative means is less developed. We will treat solutions of N_2 in progressively higher densities of Ar at 298 K, well above the critical temperature[38] of 151 K, and finally in liquid Ar.

Work of others which relates to these solution studies includes that of Bratos and Marechal[39] and Bratos and Leicknam,[40] who treated Raman band shapes in solution from a correlation function viewpoint, including solvent effects in a stochastic approach. Levesque, Weis, and Oxtoby[41] have treated the vibrational dephasing aspect in liquid N_2 and Knauss[42] has studied diatomics in solvent. Clarke, Miller, and Woodcock[43] have computed liquid N_2

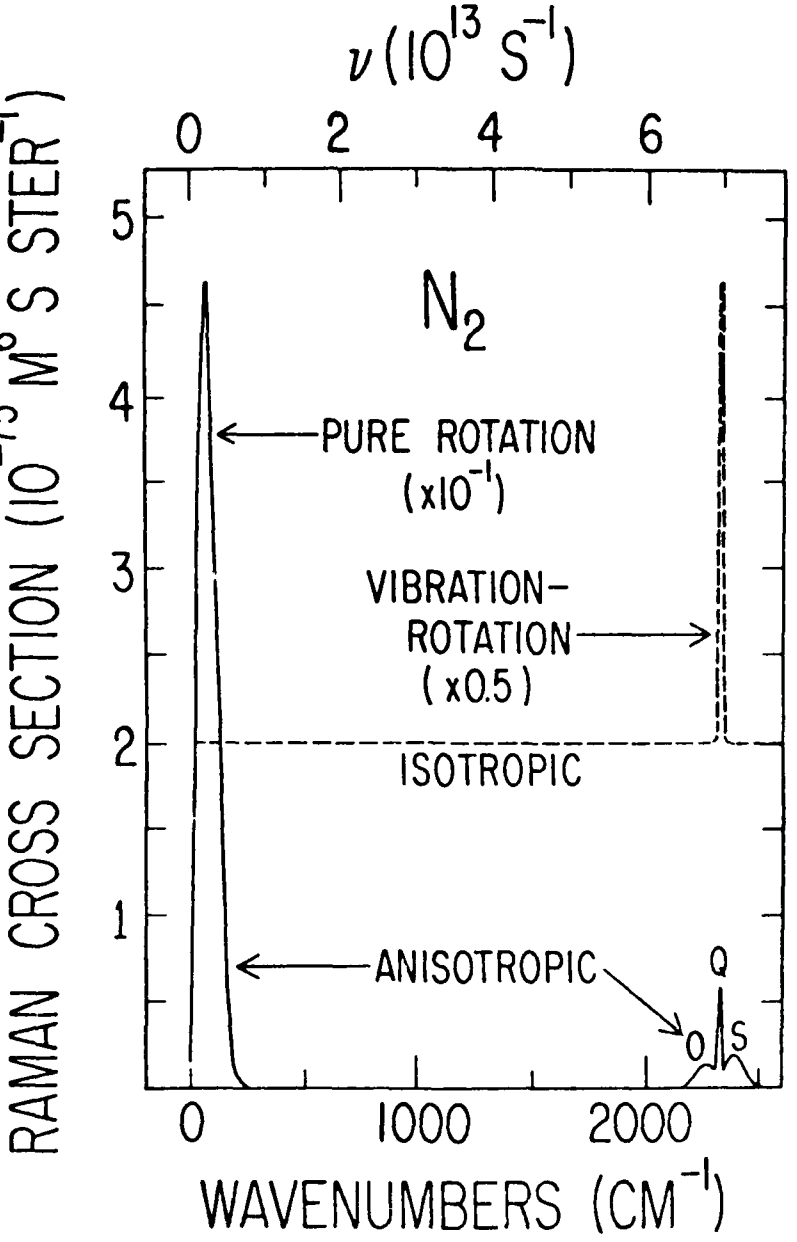

FIG. 1. Isotropic and anisotropic Raman spectra for gas phase N_2 at 298 K, showing the quantum band contours which we will examine in subsequent figures in more detail. The rotational lines are broadened to 18 cm^{-1} full-width at half maximum Gaussians to allow the different features to be seen on a similar scale. The isotropic spectrum shows no pure rotational scattering and only Q branch ($\Delta J=0$) vibrational-rotational scattering. The anisotropic spectrum shows pure rotational scattering and O ($\Delta J=-2$), S ($\Delta J=+2$) as well as Q branch vibrational-rotational scattering. The Raman wavelength weighted differential cross section, $\bar{\nu}_s^4 \frac{d^2\sigma}{d\omega d\Omega}$, in units of m^6 s steradian^{-1} shown on the vertical axis in this and subsequent figures is scaled appropriately for the upper horizontal axis in units of frequency ν in s^{-1}, but not for the lower axis of wavenumbers in cm^{-1} nor for the units of angular frequency ω in rad s^{-1} used in the theoretical discussion.

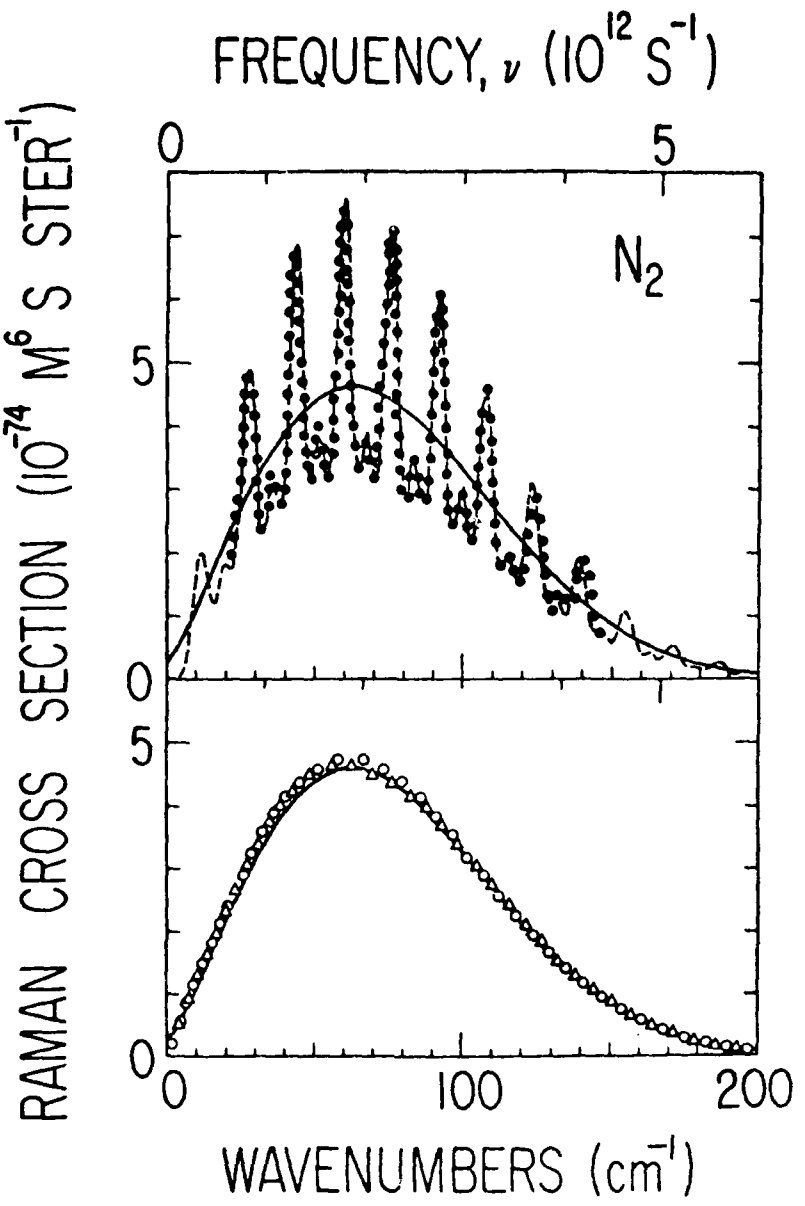

FIG. 2. Rotational anisotropic Raman spectra for dilute gas phase pure N_2 at 298 K. In the upper panel, the dashed line shows the gas phase computed quantum rotational anisotropic spectrum with the lines broadened so that they can be compared with the experimental spectrum, shown as solid circles, of De Santis, *et. al.* in 19 amagat (20 atm) N_2. The experimental spectrum is given in arbitrary cross section units and we have normalized it to the computed spectrum. The solid line is the quantum band contour, calculated by further broadening the lines of the computed spectrum until they merge. The intensity alternation in the lines is from the statistical weights of the nuclear spin states. The lower panel repeats the quantum spectrum as a solid line and compares it with open circles showing the quantum corrected correspondence limit classical band contour and open triangles showing the quantum corrected Newtonian (classical molecular dynamics, classical linear response, and classical ensemble average) spectrum. The Newtonian spectrum is averaged over 30000 single-molecule 24.6×10^{-12} s time histories, with a 5×10^{-16} s integration step, run in groups of 300 non-interacting molecules. The isotropic rotational Raman spectra are not shown as they are zero.

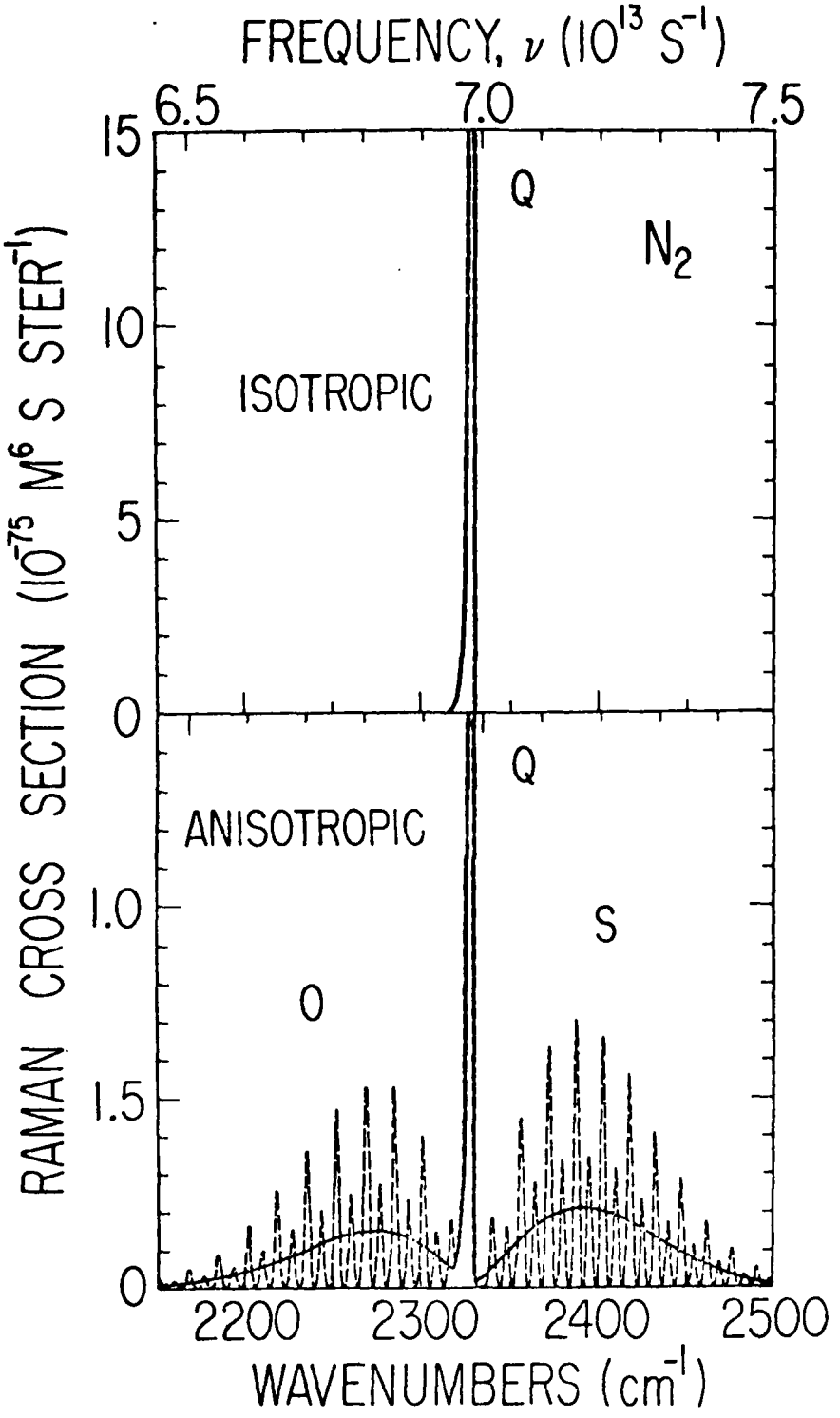

FIG. 3. Fundamental vibrational-rotational Raman spectra for dilute gas phase N_2 at 298 K. The upper panel shows the isotropic cross section and the lower panel shows the anisotropic cross section. The dashed line shows the computed quantum spectrum, with the lines partially broadened. The solid line is the quantum band contour produced by further broadening the individual vibrational-rotational lines until they merge.

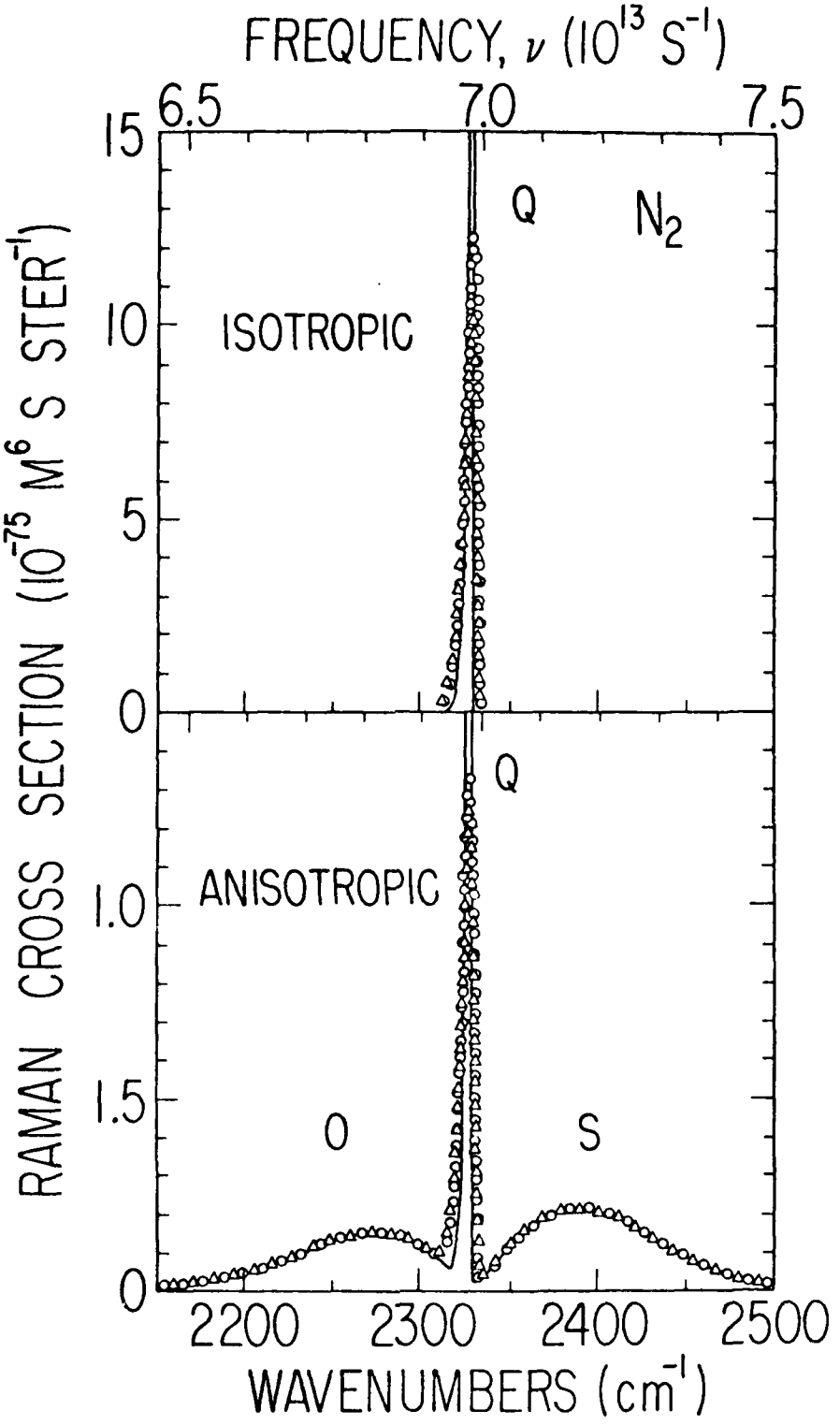

FIG. 4. Fundamental vibrational-rotational Raman spectral band contours for dilute gas phase N_2 at 298 K. The solid line is the computed quantum band contour, from Fig. 3. The open circles show the quantum corrected correspondence limit classical spectra and the open triangles show the quantum corrected Newtonian spectra. The Newtonian spectra are an average over an ensemble of 30 000 single-molecule 24.6×10^{-12} s time histories.

molecular dynamics for rigid molecules and compared to Raman line shapes. Hanson and McTague[44,45] and Frenkel and McTague[46] have computed molecular dynamics for N_2 as a rigid dumbbell and have used this approach to estimate dipole induced dipole effects.

The N_2 intramolecular potential and polarizability tensor are as before. For the Ar-N_2 intermolecular potential we use a sum of pairwise atom-atom potentials between the Ar and N atoms, each of the form

$$V(R) = A\exp[-2\xi(R-R_e)] - 2B\exp[-\xi(R-R_e)] , \tag{10}$$

in which $A=5.793\times10^{-22}$ J, $B=8.256\times10^{-22}$ J, $\xi=1.51\times10^{10}$ m^{-1}, and $R_e=2.94\times10^{-10}$ m. This potential, which would be a Morse potential if $A=B$, is due to Kistemaker and de Vries,[47] and has been shown to give classical trajectory results[47,48] in reasonable agreement with experimental rotational relaxation times[47] for N_2 in Ar. The Ar-Ar interatomic potential is the Morse-spline-van der Waals (MSV) III potential of Parson, Siska and Lee.[49] For simplicity, we leave out multi-body effects in both the polarizability function (for example distortion from sphericity of the polarizability of the Argon atoms during collisions and distortion of the N_2 polarizability tensor)[46,50] and the potential function (for example the non-pairwise additive part of the potential)[51] which should be included in a more refined treatment. The Newtonian approach could also be used to study these multi-body effects (often referred to as collision-induced) by including them in the potential and polarizability functions and comparing the results with experiment.

To facilitate comparison among the various dilute gas to dense liquid examples, we have not made the appropriate local field correction which depends upon the refractive index.[52,53] To reduce edge effects in our dynamics, we use periodic boundary conditions, replicating a truncated octahedron in a space-filling solid tessellation[20] and smoothly reducing (feathering) our forces to zero over the outer 0.01 nm of the radius of the inscribed sphere to avoid discontinuities as atoms cross the boundaries. Twenty atoms of Ar are used in the unit cell. The Newtonian vibrational-rotational spectra are again corrected for the small $+5.1$ cm^{-1} shift caused by using a finite 5×10^{-16} s time step in our trajectory integration.

As can be seen in Figs. 5 and 6, there is drastic change is spectral line shape as we proceed from dilute gas phase to a density of 1000 amagats. (One amagat unit of density is the actual concentration of the particular gas at 0 C and 1 atm pressure, which would be 2.687×10^{25} molecules m^{-3} for an ideal gas.)[54] The spectral line shapes for rotation (if continued through the origin to also show the Antistokes scattering) and vibration-rotation change from the multiple peaks characteristic of gas phase free rotation to the single peaks characteristic of liquid phase hindered rotation. The statistical noise caused by averaging over a smaller ensemble of 600 samples can be seen in Fig. 5. A comparison is made in Fig. 6 with the experimental O and S branch band shapes measured by De Santis *et. al.*[36] for pure N_2 at 276 amagats, and the agreement is close, even though the solvent is N_2 instead of Ar, indicating that the line shape is not particularly sensitive to the details of the solute-solvent intermolecular potential. Note the blue shift that occurs at the 1000 amagat density, perhaps explainable by an effectively steeper vibrational potential as the N_2 is crowded up against the repulsive walls of the solvent. The evolution of these spectral band shapes with density can be compared with those computed for the infrared case in Paper I, and with the example Raman band shapes computed stochastically by Bratos and coworkers.[39,40]

D. Liquid phase

We compute Newtonian spectra for N_2 dissolved in liquid Ar and compare with the experimental anisotropic spectra of Hanson and McTague.[44,45]

In Fig. 7 we show the rotational spectra. The Newtonian calculations are made at the experimental temperatures with the experimental densities for Ar (792 amagats at 83 K and 749 amagats at 96 K), with N_2 counted as another Ar atom. To approximately match the experimental mole fractions, one N_2 is run with 28 Ar atoms in the unit cell at 83 K and one N_2 with 20 Ar atoms at 96 K, although no direct N_2–N_2 interaction is included in the potential, as the

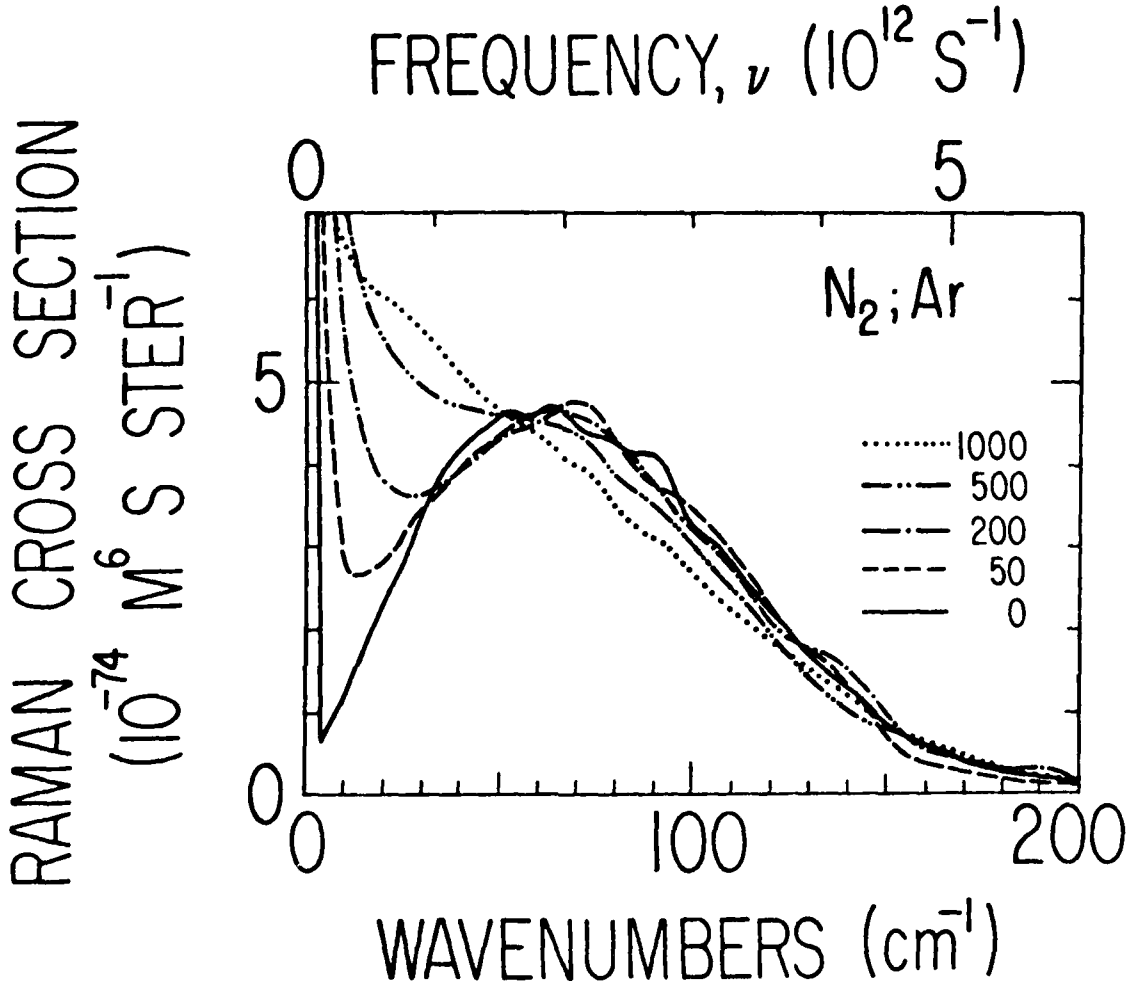

FIG. 5. Rotational Raman spectra of N_2 in different densities of Ar from 0 to 1000 amagats at 298 K. These Newtonian spectra are an average over an ensemble of 600 time histories, each lasting 24.6×10^{-12} s, for a system consisting of a single N_2 molecule surrounded by 20 Ar atoms, using periodic boundary conditions.

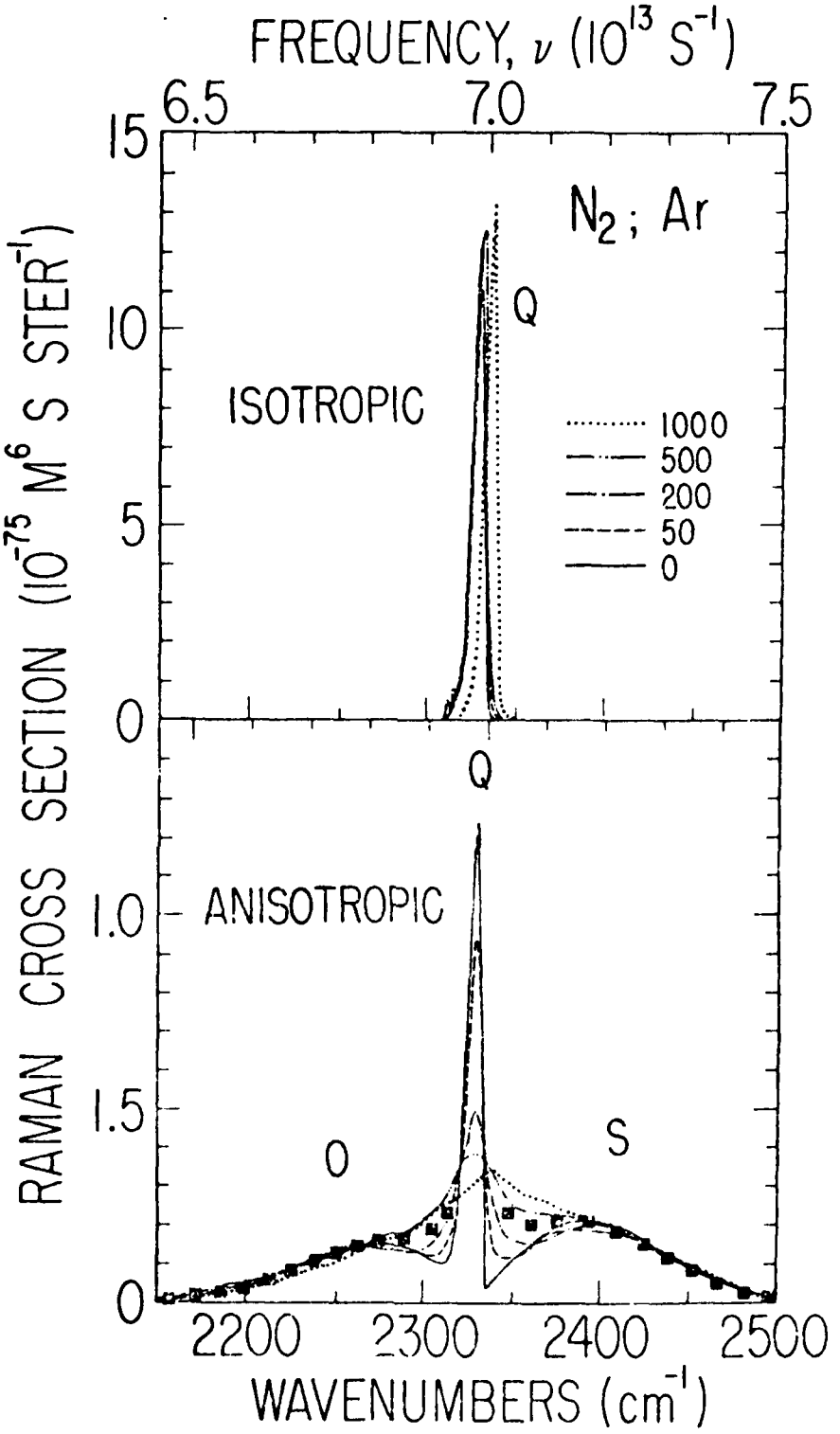

FIG. 6. Fundamental vibrational-rotational Raman spectra of N_2 in different densities of Ar from 0 to 1000 amagats at 298 K. The Newtonian spectra are computed as described in Fig. 5. A comparison is shown with the anisotropic experimental spectrum, shown as filled squares, measured by De Santis *et. al.* for pure N_2 (not in Ar) at a density of 276 amagats (365 atm) and a temperature of 296 K. The experimental spectrum is given in arbitrary cross section units and is therefore normalized to the computed spectra.

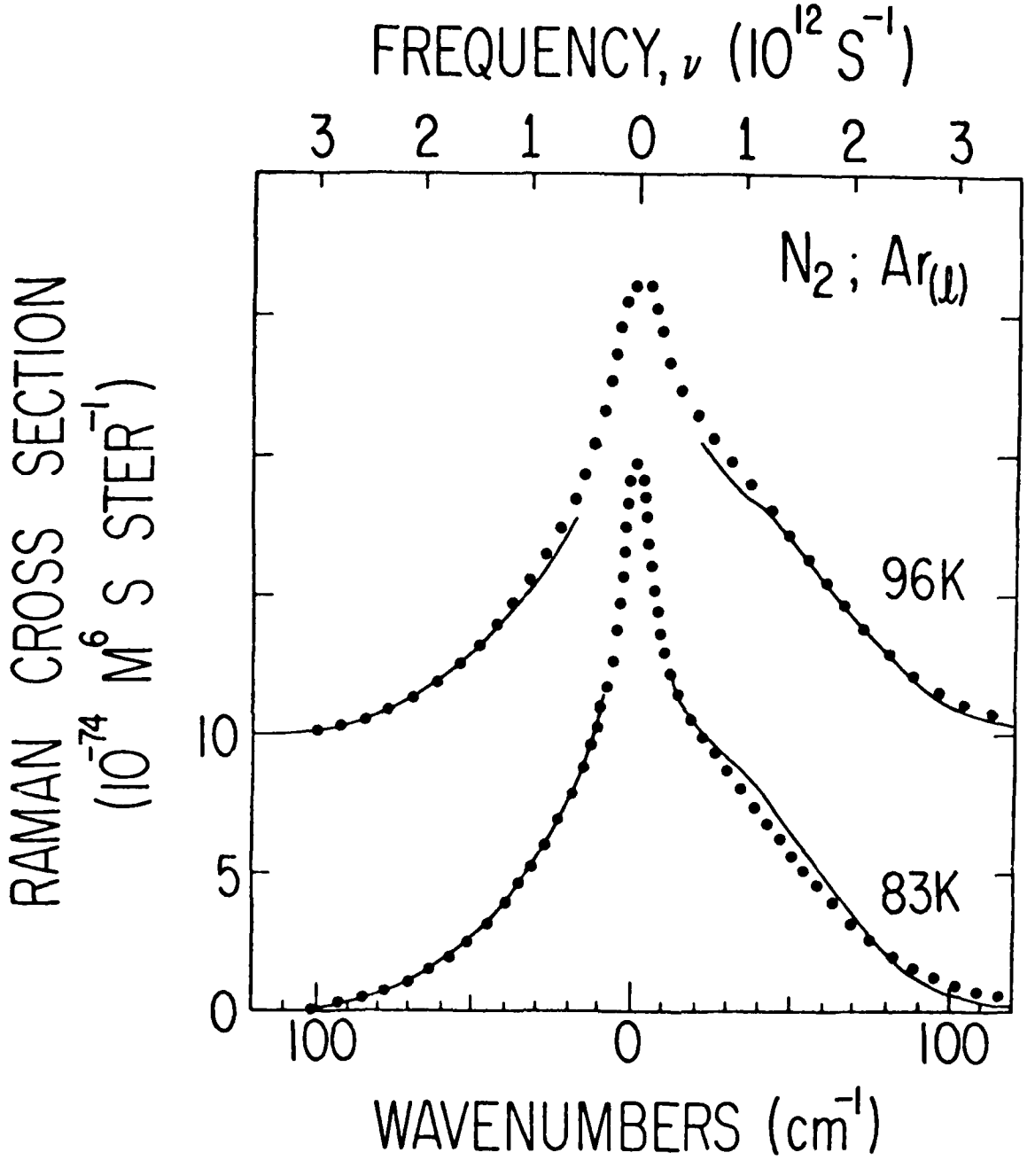

FIG. 7. Rotational Raman spectra of N_2 in liquid Ar. The Newtonian spectra, shown as solid lines, are an average over an ensemble of 200 time histories, each lasting 24.6×10^{-12} s using periodic boundary conditions, with one N_2 and 28 Ar atoms at 83 K and 20 Ar atoms at 96 K. The filled circles show the experimental spectra of Hanson and McTague, which are given in arbitrary units and thus have been normalized to the theoretical cross sections.

forces are feathered to zero before the N_2 in the adjoining periodic cell would have been felt.

The agreement of quantum corrected Newtonian calculation and experiment is seen to be quite close, but not exact. It is not known how the blame for the remaining small discrepancy should be apportioned among the *i*) inaccuracy of the potential and polarizability functions we use, in particular our neglect of multi-body (so called collision-induced effects),[46,50] *ii*) imperfection in our Newtonian methodology, *iii*) statistical noise due to inadequate ensemble sampling with only 200 runs, and *iv*) possible experimental inaccuracy.

For the vibrational-rotational fundamental band shown in Fig. 8, the agreement with the anisotropic results of Hanson and McTague is excellent except near the very peaks of the curves. This disagreement is possibly due to either inaccuracy in our theoretical approach or to the difficulty which Hanson[44] cites in accurately removing the much stronger isotropic peak which is shown in the upper panel. This experimental difficulty is compounded by the factor of one tenth in Eq. (7), which makes the ratio of parallel to perpendicular experimental intensities even greater than the ratio of isotropic to anisotropic intensities shown in Fig. 8.

IV. CONCLUSION

We have demonstrated that an essentially classical mechanical approach can be used to compute the Raman spectra of dense systems, using as an illustration N_2 in compressed Ar above the critical point (so that there is a continuous evolution from gas to liquid) and in lower temperature liquid Ar. Using potential energy $V(\mathbf{r})$ and polarizability $\bar{\mathbf{P}}(\mathbf{r})$ functions from the literature, with no adjustment of their parameters, we have achieved close agreement with the experimental spectral band contours from dilute gas to dense liquid. In addition, we find very close agreement with the quantum spectral contours for the dilute gas case in which a quantum solution can be accurately computed. Since the band shapes are derived from molecular dynamics, we can have confidence that the computed dynamics provide an accurate representation, within the limits of classical mechanics, of the actual molecular motions.

As with the molecular dynamics calculations of a number of other observables, such as transport phenomena and chemical reactions, if we average over a sufficient number of quantum states, for example in an equilibrium system at a sufficiently high temperature, so that sharp resonances are not observed, then measurables are usually reasonably well reproduced by classical mechanical calculations. We have illustrated two related ways to average over the resonances: first, lowering the resolution of observation to produce the band contour in the gas phase, and second, broadening the resonances by perturbing the stationary states at higher densities in compressed or in condensed phases.

The results in this paper and particularly in Fig. 2 of Paper I indicate that vibrational-rotational band shapes can be quite sensitive to the precise shape, *e.g.* anharmonicity, of the intramolecular potential, but that neither the rotational and vibrational-rotational band shapes nor the corresponding molecular motions are particularly sensitive to the detailed shape of the intermolecular potential for weakly bound solvent-solute systems. Evidence for this is that the band shapes are well reproduced by the rather crude potential forms we have used, and that the results for Ar versus N_2 as a solvent do not appear to be drastically different, as shown in Fig. 6.

These essentially classical calculations agree well with quantum reality for translational and rotational motions because enough states are accessible for the correspondence principle to apply. In contrast, for N_2 vibration almost the whole population at the temperatures considered is in the ground state, and thus the correspondence principle argument is not valid. However, as discussed in Paper I, molecular vibrations are ordinarily close enough to harmonic that the special parallels between classical and quantum harmonic oscillator behavior[55-58] do apply and only an amplitude correction for quantum (here zero-point) versus classical thermal motion is needed. The anharmonicity of the oscillation does not enjoy such a privileged position, and we must quantum correct our classical spectra for two anharmonic effects if we wish close agreement with experimental reality. First, a small shift (the order of a percent) in vibrational line position is necessary. Second, since a classical anharmonic oscillator vibrates in a trajectory

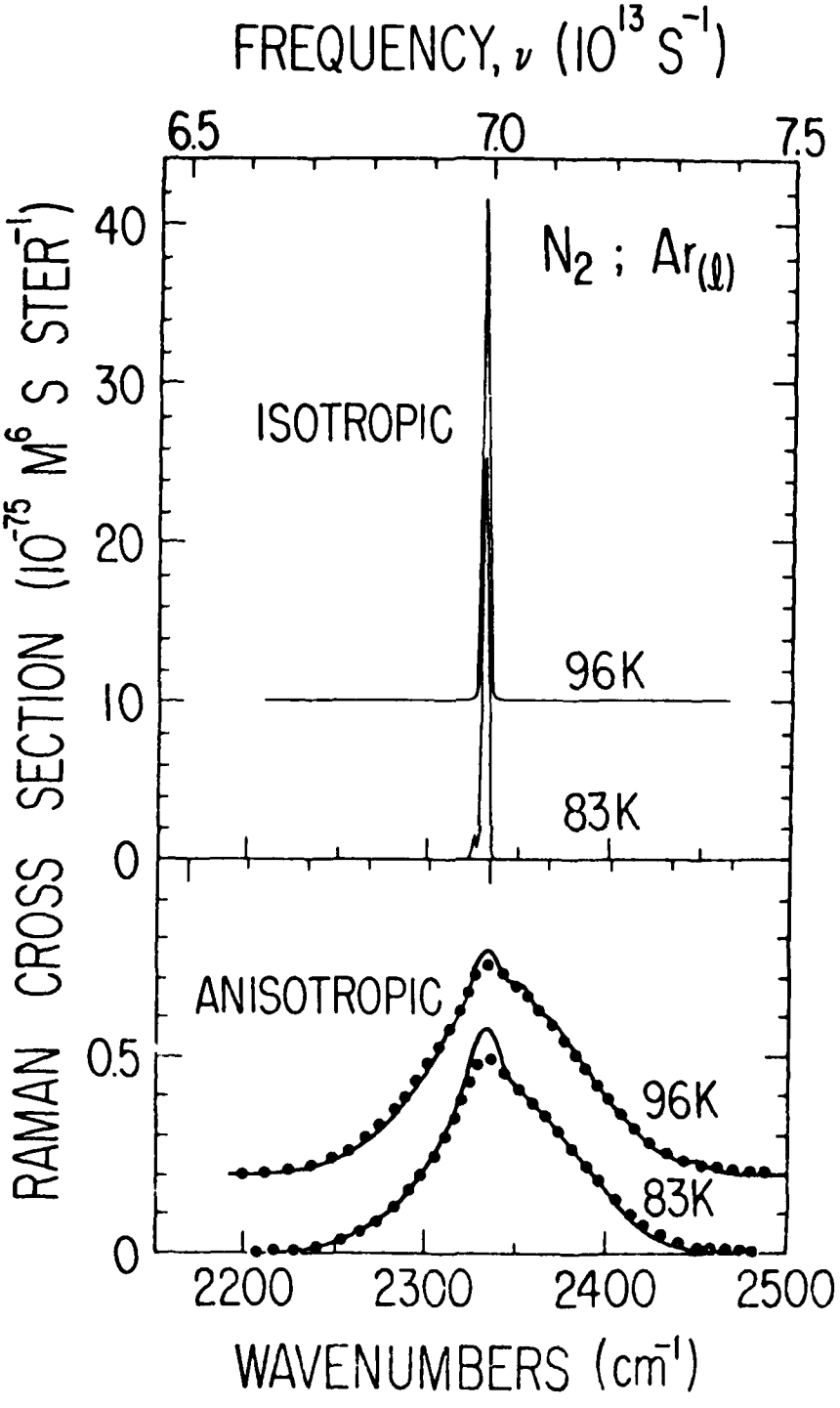

FIG. 8. Vibrational-rotational Raman spectra of N_2 in liquid Ar. The Newtonian spectra, shown as solid lines, are computed as discussed in Fig. 7. The filled circles are the anisotropic experimental results of Hanson and McTague which are given without absolute cross section units and are thus normalized to the theoretical cross sections.

which is no longer sinusoidal, its Fourier transform is broadened in frequency by the anharmonicity. In contrast, a quantum anharmonic oscillator, if it exhibits essentially only a single 1←0 transition, is shifted but not broadened. Thus, as we've seen, in the very narrow Q branch where small broadenings are observable, an additional anharmonic correction would be necessary to closely match the quantum width. Where anharmonicity becomes a dominant factor, an improved approximation using a semiclassical approach[1,3-12] may be needed.

The advantages of a classical approach to Raman spectra are several: *i*) complex molecular systems can be treated for which quantum spectral calculations are impractical, for example very large molecules, clusters, liquids, solutions, and solids, without need to resort to normal mode analysis, *ii*) the approach can be extended to treat time-dependent and non-equilibrium systems, for example to compute the Raman spectra during the course of chemical reactions even in solution, and *iii*) experimental spectra can be analyzed in terms of atomic motions with the help of classical models and of our classical intuition, and thus understood and related to molecular dynamics for more complex molecules and systems of molecules. In fact, the quantum correction transformations can be inverted to strip away the quantum aspects from an experimental spectrum, leaving behind a classical spectrum which is truly analyzable from a classical view point, in order to deduce the intra- and inter-molecular motions involved in chemical properties and processes. One further step toward a fully classical description is possible, as Miller[12] has shown, in that the radiation field itself can be treated not as a classical field, as we have implicitly done, but rather as classical harmonic oscillators.

In conclusion, the greater difficulties in computing infrared and Raman spectra appear to lie not on the side of nuclear motion, but rather on the electronic side of the Born-Oppenheimer approximation, *i.e.* in deriving as functions of nuclear positions sufficiently accurately the potential energy $V(\mathbf{r})$, the dipole moment $\boldsymbol{\mu}(\mathbf{r})$, and the polarizability tensor $\bar{\mathbf{P}}(\mathbf{r})$. Given these functions, classical techniques of molecular dynamics, linear response and ensemble averaging followed by simple quantum corrections seem capable of producing quite accurate infrared and Raman spectra for dense gases, liquids and solids (and band contours for dilute gases), although additional quantum corrections may well to be needed for features substantially affected by vibrational anharmonicity such as overtone and combination bands and other interactions among vibrational modes.[9,59]

ACKNOWLEDGEMENTS

We thank the Office of Naval Research, Chemistry, the National Science Foundation, Chemistry, and the National Institutes of Health, Division of Research Resources, for providing the support which has made this work possible. In addition, we thank Gary M. White for his help with the calculations.

APPENDIX A: LIGHT SCATTERING AND POLARIZABILITY TENSORS

The quantum mechanical expression for the wavelength weighted Raman differential scattering cross section in terms of energy into an angular frequency range $d\omega$ and a solid angle range $d\Omega$ is given in the polarizability approximation by[1,13]

$$\lambda^4 \frac{d^2\sigma}{d\omega d\Omega} = \sum_i \rho_i \sum_f |\langle f|\hat{\boldsymbol{\epsilon}}'\cdot\bar{\mathbf{P}}\cdot\hat{\boldsymbol{\epsilon}}''|i\rangle|^2 \delta(\omega_f - \omega) \qquad (A1)$$

in which $2\pi\lambda$, is the wavelength of the scattered radiation, ρ_i is the probability that the system is in the initial state i, $\hat{\boldsymbol{\epsilon}}'$ and $\hat{\boldsymbol{\epsilon}}''$ are unit vectors in the directions of the electric vectors of the incident and scattered radiation, respectively, $\bar{\mathbf{P}}$ is the space fixed Cartesian polarizability tensor of the system of molecules, and $\omega_f = (E_f - E_i)/\hbar$, where E_f and E_i are the energies of the final and initial states, respectively.

The Cartesian polarizability tensor $\bar{\mathbf{P}}$ can be represented as the 3×3 matrix $\bar{P}_{ij}$, where i and j are each one of the space fixed axes x, y, or z. This tensor can be decomposed into a diagonal isotropic tensor and a traceless anisotropic tensor.

$$\bar{\mathbf{P}} = \bar{\mathbf{P}}_{iso} + \bar{\mathbf{P}}_{aniso} \tag{A2}$$

in which

$$\bar{\mathbf{P}}_{iso} = \tfrac{1}{3} Tr\, \bar{\mathbf{P}} = \alpha_{iso}\, \mathbf{I} \tag{A3}$$

and

$$\bar{\mathbf{P}}_{aniso} = \bar{\mathbf{P}} - \bar{\mathbf{P}}_{iso} = \bar{\mathbf{P}} - \alpha_{iso}\, \mathbf{I}\,, \tag{A4}$$

I being the unit tensor and Tr indicating the trace. From these two tensors we may define two polarizability rotational invariants, α_{iso} and α_{aniso}, which measure the isotropy and anisotropy, respectively, as

$$\tfrac{1}{3} Tr\,[\bar{\mathbf{P}}_{iso}\bar{\mathbf{P}}_{iso}] = \alpha_{iso}^2 = a^2 \tag{A5}$$

and, for any symmetric polarizability tensor,

$$Tr\,[\bar{\mathbf{P}}_{aniso}\bar{\mathbf{P}}_{aniso}] = \alpha_{aniso}^2 = \tfrac{2}{3}\gamma^2 \tag{A6}$$

in which a and γ are the more usual spectroscopic notation[22] and

$$\alpha_{iso} = \tfrac{1}{3}(\bar{P}_{xx} + \bar{P}_{yy} + \bar{P}_{zz}) \tag{A7}$$

$$\alpha_{aniso} = \tfrac{1}{3}[(\bar{P}_{xx} - \bar{P}_{yy})^2 + (\bar{P}_{yy} - \bar{P}_{zz})^2 + (\bar{P}_{zz} - \bar{P}_{xx})^2 + 6(\bar{P}_{xy}^2 + \bar{P}_{xz}^2 + \bar{P}_{zx}^2)]\,. \tag{A8}$$

For a diatomic molecule with polarizability expressed in molecule fixed coordinates with the z axis along the internuclear axis, $\bar{P}_{xx}=\bar{P}_{yy}$ and all the off diagonal polarizability components are zero. Thus, for a diatomic, Eqs. (A7) and (A8) in molecule fixed coordinates simplify to

$$\alpha_{iso} = \tfrac{1}{3}(\bar{P}_{zz} + 2\bar{P}_{xx}) \tag{A9}$$

$$\alpha_{aniso}^2 = \tfrac{2}{3}(\bar{P}_{zz} - \bar{P}_{xx})^2\,. \tag{A10}$$

We can write

$$\left(\pi^4 \frac{d^2\sigma}{d\omega d\Omega}\right)_{iso} = \sum_{i,f} \rho_i\, |<f|\bar{\mathbf{P}}_{iso}|i>|^2\, \delta(\omega_{fi}-\omega) \tag{A11}$$

$$\left(\pi^4 \frac{d^2\sigma}{d\omega d\Omega}\right)_{aniso} = \sum_{i,f} \rho_i\, |<f|\bar{\mathbf{P}}_{aniso}|i>|^2\, \delta(\omega_{fi}-\omega)\,. \tag{A12}$$

the isotropic and anisotropic Raman wavelength weighted cross sections, respectively.

In order to avoid the awkward properties of the Cartesian tensor $\bar{\mathbf{P}}$ under rotational transformations, we introduce tensors that transform properly.[60] We construct a unitary transformation,[61] represented by the unitary 9×9 matrix U, the components of which are shown in Table III.

TABLE III. Components of the U matrix

	$\bar{P}_{xx}$	$\bar{P}_{yy}$	$\bar{P}_{zz}$	$\bar{P}_{xz}$	$\bar{P}_{zx}$	$\bar{P}_{yz}$	$\bar{P}_{zy}$	$\bar{P}_{xy}$	$\bar{P}_{yx}$
$P_0^{(0)}$	$-\frac{1}{\sqrt{3}}$	$-\frac{1}{\sqrt{3}}$	$-\frac{1}{\sqrt{3}}$	0	0	0	0	0	0
$P_1^{(1)}$	0	0	0	$-\frac{1}{2}$	$\frac{1}{2}$	$-\frac{i}{2}$	$\frac{i}{2}$	0	0
$P_0^{(1)}$	0	0	0	0	0	0	0	$\frac{-i}{\sqrt{2}}$	$-\frac{-i}{\sqrt{2}}$
$P_{-1}^{(1)}$	0	0	0	$-\frac{1}{2}$	$\frac{1}{2}$	$\frac{i}{2}$	$-\frac{i}{2}$	0	0
$P_2^{(2)}$	$\frac{1}{2}$	$-\frac{1}{2}$	0	0	0	0	0	$\frac{i}{2}$	$\frac{i}{2}$
$P_1^{(2)}$	0	0	0	$-\frac{1}{2}$	$-\frac{1}{2}$	$-\frac{i}{2}$	$-\frac{i}{2}$	0	0
$P_0^{(2)}$	$-\frac{1}{\sqrt{6}}$	$-\frac{1}{\sqrt{6}}$	$\frac{2}{\sqrt{6}}$	0	0	0	0	0	0
$P_{-1}^{(2)}$	0	0	0	$\frac{1}{2}$	$\frac{1}{2}$	$-\frac{i}{2}$	$-\frac{i}{2}$	0	0
$P_{-2}^{(2)}$	$\frac{1}{2}$	$-\frac{1}{2}$	0	0	0	0	0	$-\frac{i}{2}$	$-\frac{i}{2}$

U transforms the Cartesian tensor $\bar{\mathbf{P}}$ when written as the 9×1 vector

$$\bar{\mathbf{P}} = [\bar{P}_{xx}\ \bar{P}_{yy}\ \bar{P}_{zz}\ \bar{P}_{xz}\ \bar{P}_{zx}\ \bar{P}_{yz}\ \bar{P}_{zy}\ \bar{P}_{xy}\ \bar{P}_{yx}]^{\mathrm{T}} \tag{A13}$$

into the spherical tensor $\mathbf{P}$. T indicates the transpose. $\mathbf{P}$ can be resolved into three spherical irreducible tensors

$$\mathbf{P} = \mathbf{P}^{(0)} + \mathbf{P}^{(1)} + \mathbf{P}^{(2)} \tag{A14}$$

whose components $P_m^{(j)}$ are for $\mathbf{P}^{(0)}$,

$$P_0^{(0)} = -\tfrac{1}{\sqrt{3}}(\bar{P}_{xx} + \bar{P}_{yy} + \bar{P}_{zz})\ , \tag{A15}$$

for $\mathbf{P}^{(1)}$,

$$P_{+1}^{(1)} = \tfrac{1}{2}[\bar{P}_{zx} - \bar{P}_{xz} \pm (i\,\bar{P}_{zy} - i\,\bar{P}_{yz})] \tag{A16}$$

$$P_0^{(1)} = \tfrac{1}{\sqrt{2}}(i\,\bar{P}_{xy} - i\,\bar{P}_{yx})\ , \tag{A17}$$

and for $\mathbf{P}^{(2)}$,

$$P_{+2}^{(2)} = \tfrac{1}{2}(\bar{P}_{xx} - \bar{P}_{yy} \pm i\,\bar{P}_{xy} \pm i\,\bar{P}_{yx}) \tag{A18}$$

$$P_{+1}^{(2)} = -\tfrac{1}{2}(\pm\bar{P}_{xz} \pm \bar{P}_{zx} + i\,\bar{P}_{yz} + i\,\bar{P}_{zy}) \tag{A19}$$

$$P_0^{(2)} = \tfrac{1}{\sqrt{6}}(2\bar{P}_{zz} - \bar{P}_{xx} - \bar{P}_{yy})\ . \tag{A20}$$

as can be verified by the relations

$$\mathbf{P} = \mathbf{U}\,\bar{\mathbf{P}} \tag{A21}$$

$$\bar{\mathbf{P}} = \mathbf{U}^{-1}\,\mathbf{P} \tag{A22}$$

in which

$$\mathbf{U}^{-1} = (\mathbf{U}^{\mathrm{T}})^{*}\ , \tag{A23}$$

the asterisk indicating the complex conjugate. We can now see that the tensor $\mathbf{P}$ consists of three irreducible tensorial sets, one of rank 0 with 1 component, one of rank 1 with 3 components, and one of rank 2 with 5 components. If the polarizability tensor for the system is symmetric (*viz.*, $P_{\mu} = P_{\mu}$) it can be seen from Eqs. (A16) and (A17) that all of the components of $\mathbf{P}^{(1)}$, the irreducible tensorial set of rank one, are zero.

We can now use Eq. (A22) to show that

$$\bar{\mathbf{P}}_{iso} = \mathbf{U}^{-1}\,\mathbf{P}^{(0)} = \mathbf{U}^{-1}\,[P_0^{(0)}\ 0\ 0\ 0\ 0\ 0\ 0\ 0\ 0]^{\mathrm{T}}$$
$$= -\tfrac{1}{\sqrt{3}}\,P_0^{(0)}\,\mathbf{I} = \tfrac{1}{3}(\bar{P}_{xx}+\bar{P}_{yy}+\bar{P}_{zz})\,\mathbf{I} \tag{A24}$$

in agreement with Eq. (A3) and

$$\bar{\mathbf{P}}_{aniso} = \mathbf{U}^{-1}\,\mathbf{P}^{(2)} = \mathbf{U}^{-1}\,[0\ 0\ 0\ 0\ P_2^{(2)}\ P_1^{(2)}\ P_0^{(2)}\ P_{-1}^{(2)}\ P_{-2}^{(2)}]^{\mathrm{T}}$$
$$= \bar{\mathbf{P}} - \mathbf{U}^{-1}\mathbf{P}^{(0)} = \bar{\mathbf{P}} - \bar{\mathbf{P}}_{iso} \tag{A25}$$

in agreement with Eq. (A4). Using Eqs. (A24) and (A25) with Eqs. (A11) and (A12), we have

$$\left(\pi_s^4\,\frac{d^2\sigma}{d\omega d\Omega}\right)_{iso} = \tfrac{1}{3}\sum_{i,f}\rho_i\,|\langle f|P_0^{(0)}|i\rangle|^2\,\delta(\omega_{fi}-\omega) \tag{A26}$$

$$\left(\pi_s^4\,\frac{d^2\sigma}{d\omega d\Omega}\right)_{aniso} = \sum_{i,f}\rho_i\sum_{m=-2}^{2}|\langle f|P_m^{(2)}|i\rangle|^2\,\delta(\omega_{fi}-\omega)\ . \tag{A27}$$

These two equations can be represented by

$$\left(\pi_s^4\,\frac{d^2\sigma}{d\omega d\Omega}\right)_j = n_j\sum_{i,f}\rho_i\sum_{m=-j}^{j}|\langle i|P_m^{(j)}|f\rangle|^2\,\delta(\omega_{fi}-\omega) \tag{A28}$$

where it is understood that $j=0$ corresponds to the isotropic case with $n_j=\frac{1}{3}$ and $j=2$ corresponds to the anisotropic case with $n_j=1$. It is this equation that will provide the starting point for both the Newtonian and quantum solutions that follow.

In addition, it is often convenient to expand each polarizability component in a Taylor's series in q, a molecular coordinate. In the approximation of electrical linearity, we keep only the first two terms, yielding

$$P_{ij} = P_{ij}^0 + \frac{dP_{ij}}{dq}\,q$$
$$= P_{ij}^0 + P'_{ij}\,q\ . \tag{A29}$$

Simularly, this can be extended to the polarizability invariants

$$\alpha_j = \alpha_j^0 + \alpha'_j \tag{A30}$$

where α_j is α_{iso} for $j=0$ and α_{aniso} for $j=2$.

APPENDIX B: LINEAR RESPONSE THEORY

The linear response theory of Raman spectroscopy has been developed by Gordon,[1,14,16] whose approach we follow here and also discussed by others.[17,39,62,63] The first step is to convert Eq. (A28) from the Schrödinger to the Heisenberg picture by introducing the Fourier transform of the Dirac delta function,

$$\delta(\omega) = \frac{1}{2\pi}\int_{-\infty}^{\infty}e^{i\omega t}\,dt\ . \tag{B1}$$

From Eqs. (A28) and (B1)

$$\left(\pi_s^4\,\frac{d^2\sigma}{d\omega d\Omega}\right)_j = n_j\sum_{i,f}\rho_i\sum_{m=-j}^{j}|\langle f|P_m^{(j)}|i\rangle|^2\,\frac{1}{2\pi}\int_{-\infty}^{\infty}dt\,\exp\left[\frac{(E_i-E_f)}{\hbar}-\omega\right]i\,t\ . \tag{B2}$$

Because $|i\rangle$ and $|f\rangle$ are eigenstates of the system, we have[1,17]

$$e^{-iH_f t/\hbar}\,|i\rangle = e^{-iH_{ii}t/\hbar}\,|i\rangle \tag{B3}$$

and

$$<f|\ e^{iE_f t/\hbar} = <f|\ e^{iH_o t/\hbar} \tag{B4}$$

in which H_o is the Hamiltonian in the absence of the radiation. Therefore[16]

$$\left(\pi_s^4 \frac{d^2\sigma}{d\omega d\Omega}\right)_i = \frac{1}{2\pi} \int_{-\infty}^{\infty} dt\ e^{-i\omega t}\ n_i \sum_{i,f} \rho_i \sum_{m=-j}^{j} <i|P_m^{(j)}(0)|f><f|P_m^{(j)}(t)|i> \tag{B5}$$

in which

$$P_m^{(j)}(t) = e^{iH_o t/\hbar}\ P_m^{(j)}(0)\ e^{-iH_o t/\hbar}\ . \tag{B6}$$

By closure,

$$\sum_f |f><f| = 1\ , \tag{B7}$$

and therefore

$$\left(\pi_s^4 \frac{d^2\sigma}{d\omega d\Omega}\right)_i = \frac{1}{2\pi} \int_{-\infty}^{\infty} dt\ e^{-i\omega t}\ n_i \sum_i \rho_i \sum_{m=-j}^{j} <i|P_m^{(j)}(0)P_m^{(j)}(t)|i>\ . \tag{B8}$$

Since the summation over ρ_i is just an ensemble average we can write[16]

$$\left(\pi_s^4 \frac{d^2\sigma}{d\omega d\Omega}\right)_i = \frac{1}{2\pi} \int_{-\infty}^{\infty} dt\ e^{-i\omega t}\ n_i \sum_{m=-j}^{j} <P_m^{(j)}(0)P_m^{(j)}(t)> \tag{B9}$$

where the $<>$ now indicates an ensemble average. Using Eqs. (A5)-(A6) and (A24)-(A25), Eq. (B9) can be transformed into Eqs. (2) and (3) of the text.

APPENDIX C: QUANTUM AND CORRESPONDENCE PRINCIPLE SPECTRA

Quantum mechanical expressions for the Raman cross section have been derived using various methods.[22, 61, 63-66] We will follow the irreducible tensorial set[60, 63, 67] approach used by Brodersen and coworkers[68-70] which is applicable to many molecular geometries, and we will use a somewhat more general form than needed for our $^1\Sigma$ diatomic in an attempt to clarify the extension to more complex molecules. Rigid rotor harmonic oscillator transition probabilities will be used, but energies (and thus frequencies and state probabilities) will include anharmonic, centrifugal and vibrational-rotational coupling terms.

We can express the sum of the tensorial operator matrix elements in Eq. (A28) in a form which applies to either the isotropic (j=0) or anisotropic (j=2) cases as

$$G = \sum_{m=-j}^{j} |<f|P_m^{(j)}|i>|^2\ . \tag{C1}$$

If we now assume that our initial and final states are separable into vibrational and rigid symmetric top rotational states,

$$|i> = |vJKM> = |v>|JKM> \tag{C2}$$

$$<f| = <v'J'K'M'| = <v'|<J'K'M'| \tag{C3}$$

in which the quantum numbers are v for the vibration, J for the total angular momentum, K for the component along the top axis, and M for the component along the space-fixed z axis, and primes indicate the final state, then we can express G as

$$G = \sum_{m=-j}^{j} |<v'|<J'K'M'|P_m^{(j)}|JKM>|v>|^2\ . \tag{C4}$$

If the coordinate system is rotated through the Euler angles Υ, χ, Ψ to coincide with the molecule-fixed coordinates, we have[69]

$$G = \sum_{m=-j}^{j} |<v'|<J'K'M'| \sum_{k=-j}^{j} P_k^{(j)}\ D_{km}^{(j)}(-\Psi, -\chi, -\Upsilon)|JKM>|v>|^2 \tag{C5}$$

in which $D^{(J)}_{km}$ are the components of the Wigner rotation matrix.[71,72] The components of $P^{(J)}_k$ are the same as those given by Eqs. (A15)-(A20) except that x, y, and z now refer to the molecule-fixed coordinates. After the rotation, $P^{(J)}_k$ is fixed along the axis of vibration and can thus be extracted from the rotational matrix element[69]

$$G = \sum_{m=-J}^{J} \left| \sum_{k=-j}^{j} <v'|P^{(J)}_k|v><J'K'M'|D^{(J)}_{km}(-\Psi,-\chi,-\Upsilon)|JKM>\right|^2 . \tag{C6}$$

The absolute value squared of the rotational matrix element can be summed over M', m and M symmetrically using Wigner 3j symbols[73]

$$\sum_{M,m,M} |<J'K'M'|D^{(J)}_{km}|JKM>|^2 = (2J'+1)(2J+1)\begin{pmatrix} J' & j & J \\ -K' & k & K \end{pmatrix}^2$$

$$= (2J+1)\, C(JjJ';K\Delta K)^2 \tag{C7}$$

$C(JjJ';K\Delta K)$ is the Clebsch-Gordan coefficient for the coupling of angular momentum and is tabulated for the appropriate cases elsewhere.[68] It vanishes unless the selection rules[68]

$$K' - K = \Delta K = k \tag{C8}$$

$$|J - j| \leqslant J' \leqslant J + j \tag{C9}$$

and

$$J'-J \text{ even, if } K=K'=0 \tag{C10}$$

are fulfilled. Thus from Eqs. (A28), (C1), (C6), and (C7),

$$\left(\bar{\nu}_s^4 \frac{d^2\sigma}{d\omega d\Omega}\right)_J = n_i \sum_j \rho_j\, g\, |<v'|P^{(J)}_{\Delta K}|v>|^2\, (2J+1)\, C(JjJ';K\Delta K)^2\, \delta(\omega_{v'v}-\omega) , \tag{C11}$$

in which a degeneracy factor g is introduced which depends on the symmetry of the molecule. For our $^1\Sigma$ homonuclear diatomic, g is g_J, the nuclear spin statistical degeneracy. Since $\Delta K=0$, only Eqs. (A15) for the isotropic and (A20) for the anisotropic scattering contribute after the polarizability operators have been rotated to internal coordinates. For a diatomic, using Eqs. (A9) and (A10) and that n_i is $\frac{1}{3}$ for $J=0$ and 1 for $J=2$ we can replace $\frac{1}{\sqrt{3}}P^{(0)}_0$ with $\alpha_{v'v}$ and $P^{(2)}_0$ with $\alpha_{J'J;v'v}$. Eq. (C11) now becomes

$$\left(\bar{\nu}_s^4 \frac{d^2\sigma}{d\omega d\Omega}\right) = \sum_J \rho_J\, g_J\, |<v'|\alpha_J|v>|^2\, (2J+1)\, C(JjJ';K0)^2\, \delta(\omega_{v'v}-\omega) , \tag{C12}$$

with the isotropic cross section being given by $J=0$ and $\alpha_J=\alpha_{v'v}$ and the anisotropic by $J=2$ and $\alpha_J=\alpha_{J'J;v'v}$.

If we use the linear expansion of α_J given in Eq. (A30), the vibrational matrix element for harmonic oscillator wavefunctions is given by[74]

$$<v'|\alpha'_J + \alpha'_J\, q|v> = \alpha'_J \delta_{v',v} + \alpha'_J \left[\frac{\hbar(v+1)}{2\omega_0 m_r}\right]^{\frac{1}{2}} \delta_{v',v+1} , \tag{C13}$$

in which ω_0 is the angular frequency for the $v+1 \leftarrow v$ transition and m_r is the reduced mass.

Using Eqs. (C12) and (C13) and the Clebsch-Gordan coefficient $C(J0J';00)=1$ along with the values of the other Clebsch-Gordan coefficients given in Table IV, we can now obtain expressions for the the pure rotational and vibrational-rotational differential cross sections. For a pure rotational cross section we have $\Delta v=0$. The anisotropic rotational S ($\Delta J=+2$) branch is given by

$$\left(\bar{\nu}_s^4 \frac{d^2\sigma}{d\omega d\Omega}\right)_{J'J;v'v} = \sum_{v,J} \rho(v,J)\, (\alpha''_{J'J;v'v})^2\, \frac{3(J+1)(J+2)}{2(2J+3)}\, \delta\left[\frac{E(v,J+2)-E(v,J)}{\hbar} - \omega\right] . \tag{C14}$$

The isotropic pure rotational cross section for the S branch is zero.

TABLE IV. Pertinent squared Clebsch-Gordan coefficients

ΔJ	$C(J2J';00)^2$
-2	$\frac{3J(J-1)}{2(2J-1)(2J+1)}$
0	$\frac{J(J+1)}{(2J-1)(2J+3)}$
$+2$	$\frac{3(J+1)(J+2)}{2(2J+1)(2J+3)}$

For a fundamental vibrational-rotational transition we have $\Delta v=1$. For the O ($\Delta J=-2$) branch, the isotropic cross section is zero and the anisotropic part is given by

$$\left[\kappa_s^4 \frac{d^2\sigma}{d\omega d\Omega}\right]_{aniso} = \sum_{v,J} \rho(v,J)\ (\alpha'_{aniso})^2 \left[\frac{\hbar(v+1)}{2\omega_0 m_r}\right] \frac{3J(J-1)}{2(2J-1)} \times \delta\left[\frac{E(v+1,J-2)-E(v,J)}{\hbar} - \omega\right]. \tag{C15}$$

For the Q ($\Delta J=0$) branch we have:

$$\left[\kappa_s^4 \frac{d^2\sigma}{d\omega d\Omega}\right]_{iso} = \sum_{v,J} \rho(v,J)\ (\alpha'_{iso})^2 \left[\frac{\hbar(v+1)}{2\omega_0 m_r}\right] (2J+1)\ \delta\left[\frac{E(v+1,J)-E(v,J)}{\hbar} - \omega\right] \tag{C16}$$

$$\left[\kappa_s^4 \frac{d^2\sigma}{d\omega d\Omega}\right]_{aniso} = \sum_{v,J} \rho(v,J)\ (\alpha'_{aniso})^2 \left[\frac{\hbar(v+1)}{2\omega_0 m_r}\right] \frac{(2J+1)J(J+1)}{(2J-1)(2J+3)} \times \delta\left[\frac{E(v+1,J)-E(v,J)}{\hbar} - \omega\right] \tag{C17}$$

And for the S ($\Delta J=+2$) branch

$$\left[\kappa_s^4 \frac{d^2\sigma}{d\omega d\Omega}\right]_{aniso} = \sum_{v,J} \rho(v,J)\ (\alpha'_{aniso})^2 \left[\frac{\hbar(v+1)}{2\omega_0 m_r}\right] \frac{3(J+1)(J+2)}{2(2J+3)} \times \delta\left[\frac{E(v+1,J+2)-E(v,J)}{\hbar} - \omega\right] \tag{C18}$$

with the isotropic cross section being zero. In Eqs. (C14)-(C18)

$$\rho(v,J) = \frac{g_J\ e^{-\beta E(v,J)}}{\sum_{v=0}^{\infty}\sum_{J=0}^{\infty} g_J\ (2J+1)\ e^{-\beta E(v,J)}} \tag{C19}$$

where the sums in Eqs. (C14)-(C19) are over all the initial vibrational and rotational states.

The final approximation is to use energy levels evaluated to second order in perturbation theory, involving the third and fourth derivatives of the potential, giving[75]

$$E(v,J) = h\left[\nu_e(v+\tfrac{1}{2}) + B_e J(J+1) - \nu_e x_e (v+\tfrac{1}{2})^2 - \alpha_e (v+\tfrac{1}{2}) J(J+1) - \bar{D}_e J^2 (J+1)^2\right] \tag{C20}$$

in which

$$B_e = \frac{\hbar}{4\pi I_e} \tag{C21}$$

$$I_e = m_r R_e^2 \tag{C22}$$

$$\nu_e = (2\pi)^{-1}\left[\frac{V''(R_e)}{m_r}\right]^{1/2} \tag{C23}$$

$$\nu_e x_e = \frac{B_e^2 R_e^4}{4h\nu_e^2}\left[\frac{10B_e R_e^2[V'''(R_e)]^2}{3h\nu_e^2} - V''''(R_e)\right] \tag{C24}$$

$$\alpha_e = \frac{-2B_e^2}{\nu_e}\left[\frac{2B_e R_e^3 V'''(R_e)}{h\nu_e^2} + 3\right] \tag{C25}$$

and

$$\bar{D}_e = \frac{4B_e^3}{\nu_e^2}. \tag{C26}$$

In the above, $V''(R_e)$, $V'''(R_e)$ and $V''''(R_e)$ are the second, third and fourth derivatives of the internuclear potential at the bond length R_e of the potential minimum.

All three of the above approximations (linearity of the polarizability, rigid rotor harmonic oscillator evaluation of the transition matrix-elements, and energy level evaluation by second order perturbation theory through third and fourth derivatives of the potential function) may be extended to higher terms to give higher accuracy.[65, 76-78]

Using these formulas, we can evaluate the quantum spectrum, and then obtain the band contours by broadening the δ functions, for example, into Gaussians

$$\delta(\omega_{fi}-\omega) \rightarrow (\Lambda/\pi)^{1/2}\exp[-\Lambda(\omega_{fi}-\omega)^2] , \tag{C27}$$

letting Λ decrease until the individual rotational peaks merge.

By evaluating Eqs. (C14)-(C26) at successively lower values of Planck's constant, until the resulting functions converge to a limit, we can compute the correspondence principle classical differential cross section. Our Newtonian calculations, with sufficient runs to form a reliable ensemble sample, should converge to these correspondence principle results. Slight deviations can result from the approximations in Eqs. (C14)-(C26), but they should be negligible in the present context.

APPENDIX D: SEPARATION OF VIBRATION AND ROTATION

We have already made the approximation of separability of vibrational and rotational states as far as the transition matrix elements. If we make the further approximation of separability for the energy levels, we can write the Raman cross sections as convolutions of vibrational and rotational cross sections. If we use Eq. (C11), and if we consider a vibrational-rotational transition corresponding to a particular ΔK, we have

$$\left[\lambda_s^4 \frac{d^2\sigma}{d\omega d\Omega}\right]_j^Q = n_i \sum_f \rho_i \, |\langle v'|P_{\Delta K}^{(j)}|v\rangle|^2 \, g_J (2J+1) \, C(JjJ';K\Delta K)^2 \delta(\omega_{fi}-\omega) , \tag{D1}$$

in which the superscript Q indicates a quantum mechanical differential cross section and $j=0$ indicates isotropic and $j=2$ anisotropic. Let

$$VIB(j) = |\langle v'|P_{\Delta K}^{(j)}|v\rangle|^2 \tag{D2}$$

and

$$ROT(j) = n_i \, g_J (2J+1) \, C(JjJ';K\Delta K)^2 . \tag{D3}$$

If we drop any coupling terms between vibration and rotation in the energy, we have

$$\begin{aligned}\hbar\omega_{fi} &= E(v',J',K') - E(v,J,K) \\ &\approx [E(v')-E(v)] + [E(J',K')-E(J,K)] = \hbar\omega_{v',v} + \hbar\omega_{J'K,JK}\end{aligned} \tag{D4}$$

where $\omega_{v',v}$ and $\omega_{J'K,JK}$ are the angular frequency differences between the vibrational states v' and v and the rotational states $J'K'$ and JK respectively. Then we can separate the density of

states into vibrational and rotational factors

$$\rho_i = \rho(\mathrm{v},J,K) = \rho(\mathrm{v})\,\rho(J,K) \tag{D5}$$

in which, for a system at equilibrium,

$$\rho(\mathrm{v}) = \frac{e^{-\beta E(\mathrm{v})}}{\sum_{\mathrm{v}} e^{-\beta E(\mathrm{v})}} \tag{D6}$$

and

$$\rho(J,K) = \frac{e^{-\beta E(J,K)}}{\sum_{J,K} e^{-\beta E(J,K)}} , \tag{D7}$$

where $\beta=(k_B T)^{-1}$, k_B is Boltzmann's constant, and T is the temperature. The angular frequency may similarly be separated, giving

$$\delta(\omega_{fi}-\omega) = \delta(\omega_{\mathrm{v}'\mathrm{v}}+\omega_{J'K',JK}-\omega) . \tag{D8}$$

Using Eqs. (D2) and (D3), we may write Eq. (D1) as

$$\left[\pi_{\mathrm{v}}^4 \frac{d^2\sigma}{d\omega d\Omega}\right]_j^Q = \left[\sum_{\mathrm{v}} \rho(\mathrm{v})\ VIB(j)\right]\left[\sum_{J,K} \rho(J,K)\ ROT(j)\right]\delta(\omega_{\mathrm{v}'\mathrm{v}}+\omega_{J'K',JK}-\omega) . \tag{D9}$$

This can be expressed as[79]

$$\left[\pi_{\mathrm{v}}^4 \frac{d^2\sigma}{d\omega d\Omega}\right]_j^Q = \left[\sum_{\mathrm{v}} \rho(\mathrm{v})\ VIB(j)\,\delta(\omega_{\mathrm{v}'\mathrm{v}}-\omega)\right] * \left[\sum_{J,K} \rho(J,K)\ ROT(j)\,\delta(\omega_{J'K',JK}-\omega)\right]$$

$$= V^Q(j) * R^Q(j) \tag{D10}$$

in which the wavelength weighted quantum differential cross section is seen to be a convolution of the quantum vibrational cross section $V^Q(j)$ and the quantum rotational cross section, $R^Q(j)$. Such separability approximations are common in correlation function analysis of vibrational-rotational spectra,[80] in which the transformation to the time domain can be made by applying the frequency convolution theorem.[23] (See Paper I for the analogous infrared case.)

APPENDIX E: QUANTUM CORRECTIONS TO CLASSICAL SPECTRA

Our original wavelength weighted cross section given in Eq. (A1), and our separated cross sections $V^Q(j)$ in Eqs. (D2) and (D10) and $R^Q(j)$ in Eqs. (C7), (D3), and (D10) all have the basic form

$$S^Q(\omega) = \sum_{i,f} \rho_i\, |<f|\mathbf{O}|i>|^2\, \delta(\omega_{fi}-\omega) \tag{E1}$$

in which $S^Q(\omega)$ is the quantum spectrum at angular frequency ω, i is the initial and f the final state, ρ_i is the probability of state i, $\mathbf{O}$ is the appropriate operator, and $\omega_{fi}=(E_f-E_i)/\hbar$, in which E_f is the final and E_i the initial state energy. If we substitute $-\omega$ for ω, interchange the subscripts i and f in Eq. (E1), and recognize that $|<f|\mathbf{O}|i>|^2=|<i|\mathbf{O}|f>|^2$ and $\delta(\omega)=\delta(-\omega)$, we then find that

$$S^Q(-\omega) = \sum_{i,f} \rho_f\, |<f|\mathbf{O}|i>|^2\, \delta(\omega_{fi}-\omega) . \tag{E2}$$

For a system at equilibrium, $\rho_i=\exp(\beta\hbar\omega_{fi})\rho_f$, and thus

$$\frac{S^Q(\omega)}{S^Q(-\omega)} = \exp(\beta\hbar\omega_{fi}) = \exp(\beta\hbar\omega) , \tag{E3}$$

which is just an expression of detailed balance. Because of the δ-functions in Eqs. (E1) and (E2), ω can replace ω_{fi}. The correspondence principle classical limit of Eq. (E3) is

$$\frac{S^C(\omega)}{S^C(-\omega)} = \lim_{\hbar\to 0} \frac{S^Q(\omega)}{S^Q(-\omega)} = 1 , \tag{E4}$$

in which the superscript C indicates classical. Eqs. (E3) and (E4) can be understood as follows. Angular frequency ω connects states in a quantum system which are $\hbar\omega$ apart and of appreciably different Boltzmann probabilities in an equilibrium system, and thus $S^Q(\omega)$ and $S^Q(-\omega)$ are related by the detailed balance factor $\exp(\beta\hbar\omega)$. In the classical correspondence limit as $\hbar\to 0$, the scattering connects states of only infinitesimally different energy $\hbar\omega$ and thus $S^C(\omega)$ and $S^C(-\omega)$ become equal. Comparison of Eqs. (E3) and (E4) suggest that one should consider the quantum correction[62,81,82]

$$\frac{S^Q(\omega)}{S^C(\omega)} = \exp(\beta\hbar\omega/2) \tag{E5}$$

which symmetrically and simply fulfills the requirements of both equations. The factor $\omega/2$ inside the exponential in Eq. (E5) arises because $S^Q(-\omega)$ and $S^Q(\omega)$, which are related by detailed balance, lie 2ω apart in angular frequency.

Under the approximation of separation of vibration and rotation, as expressed in Eq. (D10), we will quantum correct $R^Q(j)$ and $V^Q(j)$ separately, convoluting the results where appropriate.

1. Rotational correction. From Eq. (E5) above, the rotational correction is just the detailed balance factor, and

$$R^Q(j) = \exp(\beta\hbar\omega/2)\, R^C(j) . \tag{E6}$$

Thus, for a pure rotational band, we simply multiply the classical rotational band by the factor $\exp(\beta\hbar\omega/2)$.

2. Vibrational correction. For the vibration of a harmonic oscillator of angular frequency ω_0, we can evaluate the quantum vibrational cross section $V^Q(j)$ in Eq. (D10) explicitly as[83]

$$V^Q(j) = \sum_{v=0}^{\infty} \frac{\exp[-\beta(v+\tfrac{1}{2})\hbar\omega_0]}{\sum_{v=0}^{\infty}\exp[-\beta(v+\tfrac{1}{2})\hbar\omega_0]} \left[\frac{\hbar(v+1)}{2\omega_0 m_r}\right] (P_{\Delta K}^{(J)})^2\, \delta(\omega_0-\omega) \tag{E7}$$

$$= \frac{\hbar}{2\omega m_r[1-\exp(-\beta\hbar\omega)]} (P_{\Delta K}^{(J)})^2\, \delta(\omega_0-\omega) . \tag{E8}$$

$V^C(j)$, the correspondence principle $\hbar\to 0$ classical limit of Eq. (E8), is given by

$$V^C(j) = \lim_{\hbar\to 0} V^Q(j) = (2\omega^2 m_r\beta)^{-1} (P_{\Delta K}^{(J)})^2\, \delta(\omega_0-\omega) \tag{E9}$$

In the above equations, we have used the presence of the δ-function to exchange ω for ω_0. From the ratio of Eqs. (E8) and (E9)

$$V^Q(j) = \frac{\beta\hbar\omega}{1-\exp(-\beta\hbar\omega)} V^C(j) , \tag{E10}$$

giving the harmonic oscillator quantum correction for vibration.

For a vibrational-rotational band, by Eq. (D10) we need to convolve the quantum corrections given in Eqs. (E6) and (E10). The result is that to quantum correct a classically calculated vibrational-rotational band we multiply it by

$$\frac{\beta\hbar\omega\exp[\beta\hbar(\Delta\omega)/2]}{1-\exp(-\beta\hbar\omega)} \tag{E11}$$

in which $\Delta\omega$ is the displacement within the band from its rotationless center.

The effect of potential anharmonicity is essentially the same as presented in Paper I. The dominant effect is to cause a shift in the classically calculated band position to a lower quantum frequency. A simple correction consists of evaluating the angular frequency for the rotationless

(v,J) transition $(v+1,0)\leftarrow(v,0)$ first quantum mechanically as given by Eq. (C11) and then classically by reducing Planck's constant in Eq. (C11) until convergence is reached. The offset between the classical and quantum rotationless band centers can then be used to shift the entire classical vibrational-rotational isotropic and anisotropic band contours into their quantum corrected position. A rougher approximation, $-4\pi\nu_e x_e$ (in angular frequency), as discussed in Paper I, can also be used.

The narrow Q branch presents a special problem if we wish to examine it under high resolution, as there is an additional quantum line shape correction for anharmonicity which only becomes important for it. For a harmonic oscillator, the quantum and classical pure vibrational spectra are the same. The pure vibrational lines of a quantum anharmonic oscillator are variously shifted in frequency away from the single harmonic value by the anharmonicity, but not individually broadened. In contrast, the spectrum of a classical oscillator is broadened by anharmonicity, since the classical oscillation is then not purely sinusoidal, and in addition oscillators with different energies in a thermal ensemble have different frequency distributions. If, as in the case treated here, $\hbar\omega_0$ for the vibrator is high with respect to $k_B T$ so that only a single $1\leftarrow0$ quantum transition is observed, then the quantum pure vibrational spectrum will be a single narrow line shifted in frequency by the anharmonicity, while the classical pure vibrational spectrum will have a line shape considerably broadened by anharmonicity. The classical line will be less shifted by the anharmonicity because the classical oscillator samples the potential at $\sim k_B T$, while the quantum oscillator samples the potential at the considerably higher energy $\sim\hbar\omega_0$ where the effect of anharmonicity is greater. The anharmonic effect on the width of the classical and quantum pure vibrational spectra is ordinarily (*i.e.* in Q, P, R, S branches) overwhelmed by the much larger width produced by rotational broadening. For the Q branch, the rotational broadening collapses to a narrow width, the anharmonic broadening of the classical vibrational line shape becomes apparent, and a quantum line-narrowing correction for vibrational line width must be made if the quantum Q branch line shape, and not just area, is to be reproduced by a classical calculation. This could perhaps be accomplished by deconvoluting the vibrational width from the classical Q branch. The true quantum width of the $1\leftarrow0$ Q branch can also be more closely approximated classically by the artifice of computing the spectrum for a classical harmonic oscillator, in which the pure vibrational line width (ignoring collisional and radiation damping effects) collapses to a δ-function, and the remaining width is from rotational-vibrational coupling, and then shifting the line in angular frequency by $-4\pi\nu_e x_e$ to correct for the anharmonic shift. The detailed rotational shape of the Q branch, however, would not be correct, as the rotational-vibrational coupling, quantum mechanically the α_e in Eq. (C25), will be changed by omitting the anharmonicity. The sensitivity of the shape of actual (as contrasted to theoretical rigid-rotor harmonic oscillator) Q branches to anharmonicity through vibrational-rotational coupling has often been insufficiently emphasized in attempts to assign only a vibrational origin to isotropic line shapes. In conclusion, it may be asking too much of classical mechanics to exactly reproduce the shape of a very narrow quantum line like the Q branch in a system in which there are the twin obstacles to classical convergence of *i*) population in only a single vibrational quantum state and *ii*) a major role played by anharmonicity. Perhaps the introduction of aspects of quantum mechanics directly into the molecular dynamics, in other words a semiclassical approach,[1,3,12] is the better solution for this case. In the correspondence principle and Newtonian classical spectra presented here we have not made any anharmonicity quantum correction to the Q branch line shapes and thus, while the Q branch areas are essentially correct, the shapes of the correspondence principle and Newtonian Q branches are somewhat distorted from quantum reality, as can be seen in Fig. 4.

References

1. R. G. Gordon, *Adv. Magn. Reson.* **3**, 1 (1968).
2. P. H. Berens and K. R. Wilson, *J. Chem. Phys.*, in press.
3. R. G. Gordon, *J. Chem. Phys.* **45**, 1649 (1966).
4. W. B. Neilsen and R. G. Gordon, *J. Chem. Phys.* **58**, 4131 and 4149 (1973).
5. E. J. Heller, *J. Chem. Phys.* **66**, 5777 (1977).
6. S. Y. Lee and E. J. Heller, *J. Chem. Phys.* **71**, 4777 (1979).
7. D. E. Fitz and R. A. Marcus, *J. Chem. Phys.* **62**, 3788 (1975).
8. D. W. Noid and R. A. Marcus, *J. Chem. Phys.* **67**, 559 (1977).
9. D. W. Noid, M. L. Koszykowski, and R. A. Marcus, *J. Chem. Phys.* **71**, 2864 (1979).
10. W. H. Miller, *Adv. Chem. Phys.* **25**, 69 (1974).
11. N. C. Handy, S. M. Colwell, and W. H. Miller, *Faraday Disc. Chem. Soc.* **62**, 29 (1977).
12. W. H. Miller, *J. Chem. Phys.* **69**, 2188 (1978).
13. P. H. Berens and K. R. Wilson, in *Picosecond Phenomena II*, edited by R. Hochstrasser, W. Kaiser, and C. V. Shank (Springer-Verlag, Berlin, 1980).
14. R. G. Gordon, *J. Chem. Phys.* **40**, 1973 (1964).
15. R. G. Gordon, *J. Chem. Phys.* **43**, 1307 (1965).
16. R. G. Gordon, *J. Chem. Phys.* **42**, 3658 (1965).
17. D. A. McQuarrie, *Statistical Mechanics* (Harper and Row, New York, 1976) pp. 467-592.
18. D. Beeman, *J. Comput. Phys.* **20**, 130 (1976).
19. H. C. Andersen, (Private Communication), 1980.
20. D. J. Adams, in *The Problem of Long-Range Forces in the Computer Simulation of Condensed Media*, edited by D. Ceperely (National Resource for Computation in Chemistry, Berkeley, 1980) p. 13.
21. K. R. Wilson, in *Minicomputers and Large Scale Computations*, edited by P. Lykos (American Chemical Society, Washington, 1977) p. 147.
22. D. A. Long, *Raman Spectroscopy* (McGraw-Hill, New York, 1977).
23. E. O. Brigham, *The Fast Fourier Transform* (Prentice-Hall, Englewood Cliffs, 1974).
24. R. P. Futrelle and D. J. McGinty, *Chem. Phys. Lett.* **12**, 285 (1971).
25. D. W. Noid, M. L. Koszykowski, and R. A. Marcus, *J. Chem. Phys.* **67**, 404 (1977).
26. F. J. Harris, *Proc. IEEE* **66**, 51 (1978).
27. K. P. Huber and G. Herzberg, *Molecular Spectra and Molecular Structure II. Constants of Diatomic Molecules* (Van Nostrand Reinhold, New York, 1979).
28. M. A. Morrison and P. J. Hay, *J. Chem. Phys.* **70**, 4034 (1979).
29. N. J. Bridge and A. D. Buckingham, *Proc. R. Soc. London Ser. A.* **295**, 334 (1966).
30. G. D. Zeiss and W. J. Meath, *Mol. Phys.* **33**, 1155 (1977).
31. A. C. Newell and R. C. Baird, *J. Appl. Phys.* **36**, 3751 (1965).
32. R. H. Orcutt and R. H. Cole, *J. Chem. Phys.* **46**, 697 (1967).
33. P. W. Langhoff, *J. Chem. Phys.* **57**, 2604 (1972).
34. C. Asawaroengchai and G. M. Rosenblatt, *J. Chem. Phys.* **72**, 2664 (1980).
35. H. W. Schrötter and H. W. Klöckner, in *Raman Spectroscopy of Gases and Liquids*, edited by A. Weber (Springer-Verlag, Berlin, 1979) p. 123.

36. A. De Santis, M. Sampuli, P. Morales, and G. Signorelli, *Mol. Phys.* **35**, 1125 (1978).

37. J. Bendtsen, *J. Raman Spectrosc.* **2**, 133 (1974).

38. D. White, in *American Institute of Physics Handbook*, edited by D. E. Gray (McGraw-Hill, New York, 1963) p. 4-29.

39. S. Bratos and E. Marechal, *Phys. Rev. A* **4**, 1078 (1971).

40. J. C. Leicknam, *Profils des bandes Raman associées aux transitions entre états non dégénérés pour les molécules polyatomiques dissoutes dans des solvants inertes* (Thesis, Université Pierre et Marie Curie, Paris, 1979).

41. D. Levesque, J. J. Weis, and D. W. Oxtoby, *J. Chem. Phys.* **72**, 2744 (1980).

42. D. C. Knauss, *Mol. Phys.* **36**, 413 (1978).

43. J. H. R. Clarke, S. Miller, and L. V. Woodcock, in *Molecular Motions in Liquids*, edited by J. Lascombe (D. Reidel, Dordrecht, 1974) p. 495.

44. F. E. Hanson, *I. Raman Studies of the Orientational Motions of Small Diatomics Dissolved in Argon and 2. Molecular Dynamics Simulation of Rare Gas Films* (Thesis, University of California, Los Angeles, 1979).

45. F. E. Hanson and J. P. McTague, *J. Chem. Phys.* **72**, 1733 (1980).

46. D. Frenkel and J. P. McTague, *J. Chem. Phys.* **72**, 2801 (1980).

47. P. G. Kistemaker and A. E. de Vries, *Chem. Phys.* **7**, 371 (1975).

48. D. Pattengill and R. B. Bernstein, *J. Chem. Phys.* **65**, 4007 (1976).

49. J. M. Parson, P. E. Siska, and Y. T. Lee, *J. Chem. Phys.* **56**, 1511 (1972).

50. A. J. C. Ladd, T. A. Litovitz, J. H. R. Clarke, and L. V. Woodcock, *J. Chem. Phys.* **72**, 1759 (1980).

51. J. A. Barker and D. Henderson, *Rev. Mod. Phys.* **48**, 587 (1976).

52. G. Eckhardt and W. G. Wagner, *J. Mol. Spectrosc.* **19**, 407 (1966).

53. M. J. Colles and J. E. Griffiths, *J. Chem. Phys.* **56**, 3384 (1972).

54. A. S. Friedman, in *American Institute of Physics Handbook*, edited by D. E. Gray (McGraw-Hill, New York, 1963) pp. 4-158.

55. K. Gottfried, *Quantum Mechanics, Vol. I, Fundamentals* (W. A. Benjamin, New York, 1966) pp. 66-74, 256-264.

56. K. E. Holdy, L. C. Klotz, and K. R. Wilson, *J. Chem. Phys.* **52**, 4588 (1970).

57. F. F. Heidrich, K. R. Wilson, and D. Rapp, *J. Chem. Phys.* **54**, 3885 (1971).

58. E. J. Heller, *J. Chem. Phys.* **62**, 1544 (1975).

59. E. J. Heller, E. B. Stechel, and M. J. Davis, *J. Chem. Phys.* **73**, 4720 (1980).

60. U. Fano and G. Racah, *Irreducible Tensorial Sets* (Academic Press, New York, 1959).

61. J. A. Koningstein, *Introduction to the Theory of the Raman Effect* (D. Reidel, Dordrecht, 1972).

62. B. J. Berne, in *Physical Chemistry, An Advanced Treatise*, edited by D. Henderson (Academic Press, New York, 1971) Vol. VIIIB, Chap. 9.

63. B. J. Berne and R. Pecora, *Dynamic Light Scattering* (John Wiley and Sons, New York, 1976).

64. G. Placzek, in *Handbuch der Radiologie*, edited by E. Marx (Akademische Verlagsgesellschaft, Leipzig, 1934).

65. T. C. James and W. Klemperer, *J. Chem. Phys.* **31**, 130 (1959).

66. S. Bhagavantam and T. Venkatarayudu, *Theory of Groups and its Application to Physical Problems* (Academic Press, New York, 1969).

67. Y.-N. Chiu, *J. Chem. Phys.* **52**, 3641 (1970).

68. S. Brodersen, in *Raman Spectroscopy of Gases and Liquids*, edited by A. Weber (Springer-Verlag, Berlin, 1979) p. 7.

69. F. Rasmussen and S. Brodersen, *J. Mol. Spectrosc.* **25**, 166 (1968).

70. F. Hegelund, F. Rasmussen, and S. Brodersen, *J. Raman Spectrosc.* **1**, 433 (1973).

71. M. E. Rose, *Elementary Theory of Angular Momentum* (John Wiley and Sons, New York, 1957).

72. E. P. Wigner, *Group Theory* (Academic Press, New York, 1959).

73. A. R. Edmonds, *Angular Momentum in Quantum Mechanics* (Princeton Univeristy Press, Princeton, 1960).

74. L. Pauling and E. B. Wilson, *Introduction to Quantum Mechanics* (McGraw-Hill, New York, 1935).

75. I. R. Levine, *Molecular Spectroscopy* (John Wiley and Sons, New York, 1975) pp. 142-194.

76. A. D. Buckingham and A. Szabo, *J. Raman. Spectrosc.* **7**, 46 (1978).

77. R. Herman and R. F. Wallis, *J. Chem. Phys.* **23**, 637 (1955).

78. R. C. Herman and R. J. Rubin, *Astrophys. J.* **121**, 533 (1955).

79. G. A. Korn and T. M. Korn, *Mathematical Handbook for Scientists and Engineers* (McGraw-Hill, New York, 1961) pp. 742-743.

80. D. R. Jones, H. C. Andersen, and R. Pecora, *Chem. Phys.* **9**, 339 (1975).

81. P. Schofield, *Phys. Rev. Lett.* **4**, 239 (1960).

82. B. J. Berne, J. Jortner, and R. Gordon, *J. Chem. Phys.* **47**, 1600 (1967).

83. D. Steele, *Theory of Vibrational Spectroscopy* (W. B. Saunders, Philadelphia, 1971) p. 124.

P4-2/A23

472:GAN:716:te
78u472-608

TECHNICAL REPORT DISTRIBUTION LIST, GEN

	No. Copies
Office of Naval Research Attn: Code 472 800 North Quincy Street Arlington, Virginia 22217	2
ONR Branch Office Attn: Dr. George Sandoz 536 S. Clark Street Chicago, Illinois 60605	1
ONR Branch Office Attn: Scientific Dept. 715 Broadway New York, New York 10003	1
ONR Branch Office 1030 East Green Street Pasadena, California 91106	1
ONR Branch Office Attn: Dr. L. H. Peebles Building 114, Section D 666 Summer Street Boston, Massachusetts 02210	1
Director, Naval Research Laboratory Attn: Code 6100 Washington, D.C. 20390	1
The Assistant Secretary of the Navy (R,E&S) Department of the Navy Room 4E736, Pentagon Washington, D.C. 20350	1
Commander, Naval Air Systems Command Attn: Code 310C (H. Rosenwasser) Department of the Navy Washington, D.C. 20360	1
Defense Documentation Center Building 5, Cameron Station Alexandria, Virginia 22314	12
Dr. Fred Saalfeld Chemistry Division Naval Research Laboratory Washington, D.C. 20375	1
U.S. Army Research Office Attn: CRD-AA-IP P.O. Box 1211 Research Triangle Park, N.C. 27709	1
Naval Ocean Systems Center Attn: Mr. Joe McCartney San Diego, California 92152	1
Naval Weapons Center Attn: Dr. A. B. Amster, Chemistry Division China Lake, California 93555	1
Naval Civil Engineering Laboratory Attn: Dr. R. W. Drisko Port Hueneme, California 93401	1
Department of Physics & Chemistry Naval Postgraduate School Monterey, California 93940	1
Dr. A. L. Slafkosky Scientific Advisor Commandant of the Marine Corps (Code RD-1) Washington, D.C. 20380	1
Office of Naval Research Attn: Dr. Richard S. Miller 800 N. Quincy Street Arlington, Virginia 22217	1
Naval Ship Research and Development Center Attn: Dr. G. Bosmajian, Applied Chemistry Division Annapolis, Maryland 21401	1
Naval Ocean Systems Center Attn: Dr. S. Yamamoto, Marine Sciences Division San Diego, California 91232	1
Mr. John Boyle Materials Branch Naval Ship Engineering Center Philadelphia, Pennsylvania 19112	

P4-2/A25

472:GAN:716
78u472-608

TECHNICAL REPORT DISTRIBUTION LIST, GEN

	No. Copies
Dr. Rudolph J. Marcus Office of Naval Research Scientific Liaison Group American Embassy APO San Francisco 96503	1
Mr. James Kelley DTNSRDC Code 2803 Annapolis, Maryland 21402	1

P4-2/B13

472:GAN:716:1
78u472-608

TECHNICAL REPORT DISTRIBUTION LIST, 051C

	No. Copies
Dr. M. B. Denton Department of Chemistry University of Arizona Tucson, Arizona 85721	1
Dr. R. A. Osteryoung Department of Chemistry State University of New York at Buffalo Buffalo, New York 14214	1
Dr. B. R. Kowalski Department of Chemistry University of Washington Seattle, Washington 98105	1
Dr. S. P. Perone Department of Chemistry Purdue University Lafayette, Indiana 47907	1
Dr. D. L. Venezky Naval Research Laboratory Code 6120 Washington, D.C. 20375	1
Dr. H. Freiser Department of Chemistry University of Arizona Tucson, Arizona 85721	
Dr. Fred Saalfeld Naval Research Laboratory Code 6110 Washington, D.C. 20375	1
Dr. H. Chernoff Department of Mathematics Massachusetts Institute of Technology Cambridge, Massachusetts 02139	1
Dr. K. Wilson Department of Chemistry University of California, San Diego La Jolla, California	1
Dr. A. Zirino Naval Undersea Center San Diego, California 92132	1

	No. Copies
Dr. John Duffin United States Naval Postgraduate School Monterey, California 93940	1
Dr. G. M. Hieftje Department of Chemistry Indiana University Bloomington, Indiana 47401	1
Dr. Victor L. Rehn Naval Weapons Center Code 3813 China Lake, California 93555	1
Dr. Christie G. Enke Michigan State University Department of Chemistry East Lansing, Michigan 48824	1
Dr. Kent Eisentraut, MBT Air Force Materials Laboratory Wright-Patterson AFB, Ohio 45433	1
Walter G. Cox, Code 3632 Naval Underwater Systems Center Building 148 Newport, Rhode Island 02840	1

P4-2/B11

472:GAN:71e
78u472-608

TECHNICAL REPORT DISTRIBUTION LIST, 051B

	No. Copies
Professor K. Wilson Department of Chemistry, B-014 University of California, San Diego La Jolla, California 92093	1
Professor C. A. Angell Department of Chemistry Purdue University West Lafayette, Indiana 47907	1
Professor P. Meijer Department of Physics Catholic University of America Washington, D.C. 20064	1
Dr. S. Greer Chemistry Department University of Maryland College Park, Maryland 20742	1
Professor P. Delahay New York University 100 Washington Square East New York, New York 10003	1
Dr. T. Ashworth Department of Physics South Dakota School of Mines & Technology Rapid City, South Dakota 57701	1
Dr. G. Gross New Mexico Institute of Mining & Technology Socorro, New Mexico 87801	1
Dr. J. Rassner Space Science Research Center University of Missouri - Rolla Rolla, Missouri 65401	1
Dr. J. Telford University of Nevada System Desert Research Institute Lab of Atmospheric Physics Reno, Nevada 89507	1
Dr. B. Vonnegut State University of New York Earth Sciences Building 1400 Washington Avenue Albany, New York 12203	
Dr. Hank Loos Laguna Research Laboratory 21421 Stans Lane Laguna Beach, California 92651	
Dr. John Lachan University of Manchester Institute of Science & Technology P.O. Box 88 Manchester, England M601QD	

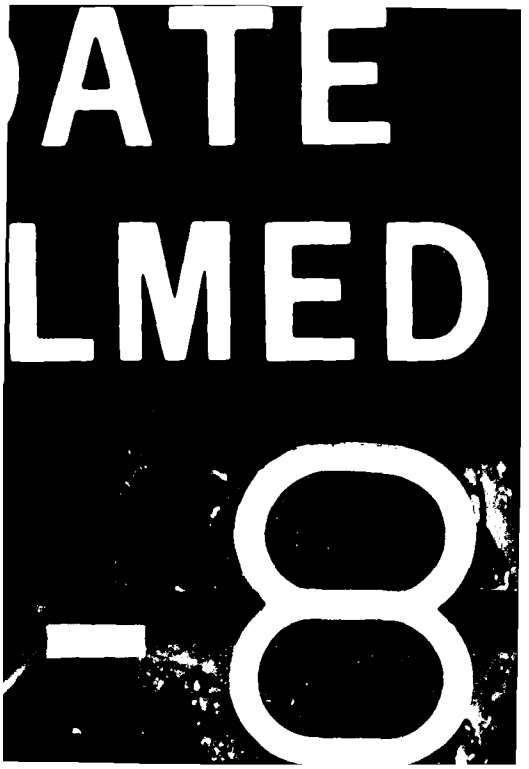
ATE
LMED
8